Department of Precision and Microsystems Engineering

Topology Optimization of Heat Exchangers

Name: Panagiotis Papazoglou

Report no	:	EM 2015.024
Coach	:	Ir. F. C. M. van Kempen
Professor	:	Dr. ir. M. Langelaar
Specialisation	:	Engineering Mechanics
Type of report	:	MSc Thesis
Date	:	24 September 2015

Delft University of Technology

Challenge the future

Topology Optimization of Heat Exchangers

by

P. Papazoglou

in partial fulfillment of the requirements for the degree of

Master of Science
in Mechanical Engineering,

at the Delft University of Technology,
to be defended publicly on Thursday September 24, 2015 at 10.30 AM.

Student number:	4321669	
Supervisor:	Dr. ir. M. Langelaar	TU Delft
	Ir. F. C. M. van Kempen	TU Delft
Thesis Committee:	Prof. dr. ir. F. van Keulen	TU Delft
	Dr. ir. M. Langelaar	TU Delft
	Ir. F. C. M. van Kempen	TU Delft
		TU Delft

Delft University of Technology

ACKNOWLEDGEMENT

At the onset, I would like to express my sincere gratitude to my supervisor, Matthijs Langelaar, for his continuous support on my thesis. On his regular supervision and his always helpful feedback.

I would like to thank my daily supervisor, Floris van Kempen, for his constant help that he provided throughout this project. During this long year he has been supporting me both in technical and psychological aspects. Moreover I would like to thank him for the time and effort he has spent on helping me write this report.

I also want to thank my friends of the PME department, for their support, help, and instant noodles they have provided.

I would finally like to thank my family and particularly my brother for all the support.

ABSTRACT

Heat exchangers have long been used in a wide variety of industrial applications, such as for energy recovery from by-products, temperature regulation in chemical processes, refrigeration, or cooling of car engines. Typically, each application requires a different type of heat exchanger such as, tube, shell, with/without phase change, mixing/non mixing etc. heat exchangers. Due to their importance, there has been an ongoing interest in reducing the operational/constructional costs and increasing the efficiency. A lot of research has be done in optimizing certain features of heat exchangers (e.g. tube dimensions, fin thickness etc.), but so far none of them investigates the optimization of the whole topology of a heat exchanger.

The aim of this thesis is to optimize the structure of a two flow heat exchanger, by means of topology optimization. More specifically we aim to maximize the efficiency of heat transfer, given some predefined pressure drop and dimension constraints. These constraints are necessitated by the need of achieving a reduced operating (pressure drop) and manufacturing (dimensions) costs. A heat exchanger, being a multi-physics system, can be described by two physical phenomena: the flow of the fluid and the heat transfer. In this study we focus on heat exchanger governed by an isothermal and incompressible Stokes flow with low Reynolds number, while the heat transfer is assumed to be advective-conductive heat transfer, without internal heat generation, characterised by a relatively high Peclet number.

We evaluate two novel models for topology optimization of heat exchangers; the Fluid Tracking Model and the Multi-Material Model. Throughout the experimental evaluation we saw that the Multi-Material Model performs best. The Fluid Tracking Model did not produce optimal results and was unable to enforce non-mixing designs. The Multi-Material Model optimized designs that maximized the heat transfer surface area between the fluids. Furthermore the designs illustrated a wall at the interfaces of the two fluids, keeping the two flows separated. Both 2D and 3D cases were studied. The 3D optimal results achieved a moderate improvement in performance over a simple design of a concentric tube heat exchanger.

Contents

1

INTRODUCTION

1.1. INTRODUCTION TO HEAT EXCHANGERS

Heat exchangers are devices that transfer thermal energy from one medium to another. They find applications in a wide variety of problems such as refrigeration, cooling, refinement, chemical processing, and they are vital parts of many industries. Although the main principle of all heat exchangers is the same, the objective, configuration and size varies greatly. For example in refrigerating systems the objective is to keep a constant temperature with the lowest possible energy loss. In contrast, chemical processes, the objective of a heat exchanger may be the maximization of the heat transfer between the two mediums while minimizing the power needed for operating. In many cases it is crucial that the process of heat transferring is done without mixing of the mediums, so that the coolant and to-be-cooled-medium do not get contaminated and can be reused without filtering.

Heat exchangers are classified on the configuration of the flowing mediums. Cross flow, counter flow, and parallel flow heat exchangers are the basic configurations that are used in common applications (see figure 1.1). This thesis focused on counter and parallel flow heat exchangers. However, in more complex geometries (see figure 5.23) such classification is not applicable.

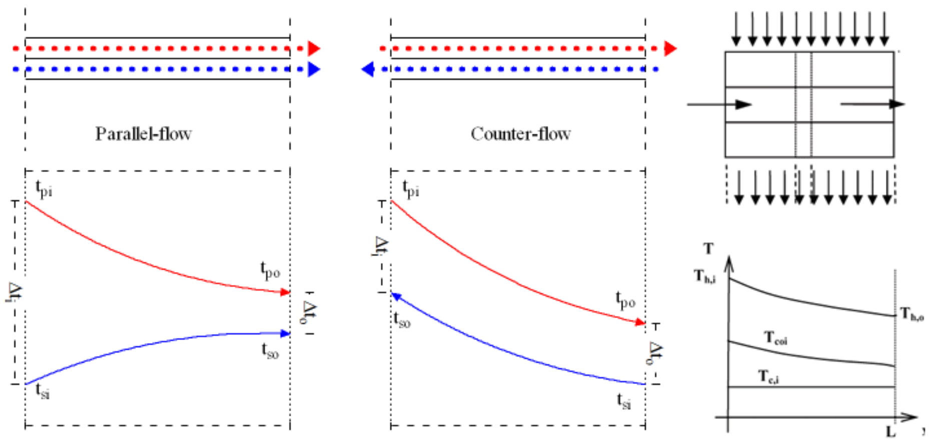

Figure 1.1: Parallel, counter and cross flow configurations of a heat exchanger, and the temperature profile of the fluids [1], [2].

1.2. PARAMETRIC OPTIMIZATION OF HEAT EXCHANGERS

In parametric models the heat exchanger has a fixed design, that is described by a finite set of parameters. An example of a parametric model is a concentric tube, where the model is fully described by five parameters: the length, diameters, thickness and material of the tubes. The optimization of these parametric models involves finding the set of parameters that optimize an objective function. Many studies have been made on the topic of parametric optimization of heat exchangers (e.g [3], [4], [5], [6], [4], [7]). By their very nature these studies are focused focused on specific types of models and applications. A characteristic example of a heat exchanger optimization study is the work of Lee et al. [4]. This study optimizes the size and spacing of the staggered pins of a plate heat exchanger. Similarly Liu et al.[6] investigated the optimal dimensions of micro-channel heat exchangers. Hadidi et al. [5] optimizes the parameters of a shell and tube heat exchanger. Many more parametric optimization problems exist, such as the optimization of the design parameters of a refrigerant systems in the work of Jain et al. [7]

Parametric models, while easy to optimize, greatly reduces the flexibility of the design, since they are described just by a few parameters. In that sense the resulted optimised design is optimal only under the geometrical constraints of the model. For example, optimizing a tube heat exchanger introduces the constraint that the channels have to be cylindrical, and does not allow for more complex channel geometries. These geometric constraints used to be a manufacturing limitation in the past, since the manufacturing of irregular shape channels was a non-trivial task. But with modern manufacturing processes (additive manufacturing), these limitations are not valid any more. Without geometrical constraints due to the manufacturing process these parametric models

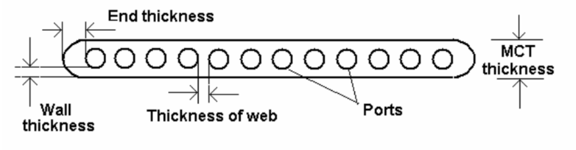

(a) Parametric optimization of a shell and tube heat exchanger [3].

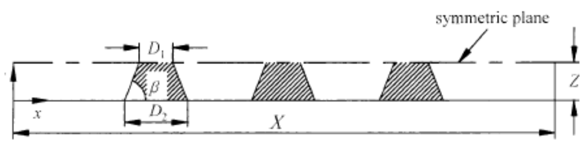

(b) Parametric optimization of the staggered pins of a plate heat exchanger [4].

Figure 1.2: Design parameters of size optimization of heat exchangers.

1.3. INTRODUCTION TO TOPOLOGY OPTIMIZATION

In order to take full advantage of the capabilities of additive manufacturing we need to be able to optimize the complete topology of a heat exchanger. Topology optimization studies the process of optimizing the topology of a domain. The term topology optimization refers to the process of finding a material distribution in space in a way that an objective is maximised. Topology optimization has been applied with success in a variety of engineering problems, such as structural problems, chemical reaction processes, electrochemical processes, flow and heat transfer problems, etc [8].

Application of topology optimization in the field of multi-flow heat exchangers is a novel idea. To the best of my knowledge, at the time of writing all research is focused on single flow problems (see Alexandersen et al. [9], Koga et al.[10], Marck et al. [11] , Borvall et al. [12], etc.). What makes multi-flow heat exchangers different than other heat transfer devices is that there is interaction between two or more fluids.

In general, due to the complexity of the geometry, a heat exchanger is studied by means of computational fluid dynamics (CFD) [13]. Each fluid flow can be studied on its own, since the geometry and boundaries are predefined, and there is no interaction between the two fluids. This is not the case for topology optimization, due to the geometry and boundaries constantly changing during the design process. This was one of the main challenges of this thesis and was a turning point for the way we proceeded in modelling the optimization problem. Another challenge that was met in this work was to keep the fluids separated by means of a solid interface wall, a property that characterises non-mixing heat exchangers. In order to prepare the reader on what to expect, an overview of the thesis is presented here:

Theoretical background of heat exchangers In this chapter we present the physical phenomena of a heat exchanger. We thoroughly look at the assumptions to make the system manageable and state the governing equations that allow us to optimize at a later stage.

Topology optimization Here we introduce the concept of topology optimization in detail. We briefly review the relevant research in topology optimization problems. We make a first attempt to optimize the topology of a heat exchanger, and discuss the challenges that we have to overcome in order to get a working model.

Fluid Tracking Model and results In this chapter we proposed an objective function and we included a fluid tracking physics to the problem, in order to satisfy these criteria: the designs must be non-mixing. Our experimental evaluations showed the short comings of this approach, which we discuss in detail.

Multi-Material Model and results In this chapter we proposed a new way of solving the flow problem, by studying each flow separately, in order to overcome the short comings of the Fluid Tracking Model. We experimentally evaluated this model and we discussed the results.

Conclusion and further research We conclude by discussing the different aspects of the two models and analysing the advantages and disadvantages, as well as making recommendations for future extensions to the Multi-Material Model, and heat exchangers in general.

2

Theoretical Background of Heat Exchangers

In this chapter we will introduce the basic concepts of heat exchangers. There exist many types of heat exchangers, depending on the application they are used. In this thesis we are going to study non-mixing heat exchangers, with no phase change, that transfer heat between two separate fluids. These kind of devices are used for cooling or heating fluids, using another fluid of lower or higher energy, respectively. The simplest example of such a device is a tube heat exchanger, consisting of two concentric tubes, where fluid flows inside them (see figure 2.1).

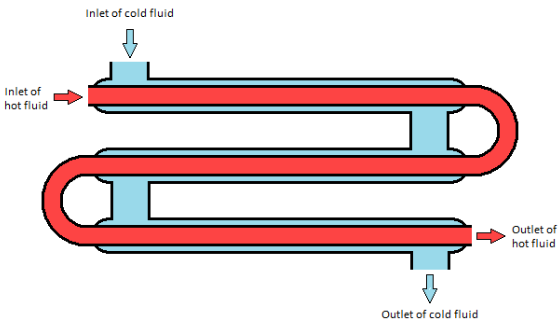

Figure 2.1: Double-pipe heat exchanger. Two fluids of different temperature flow inside concentric pipes.

Heat exchangers in general involve multiple physical phenomena, such as fluid flow, heat transfer, structural dynamics, etc. In our case we are interested in the temperature and velocity of the fluid, so we will focus on the flow and heat transfer physics of the problem.

2.1. Fluid Flow

The motion of viscous fluids can be described by the Navier-Stokes (2.1)and the mass continuity 2.2 equations:[14]

$$\frac{\partial(\rho\mathbf{u})}{\partial t}+\rho(\mathbf{u}\cdot\nabla)\mathbf{u}=\nabla\cdot\boldsymbol{\tau}-\nabla p+\mathbf{f}, \tag{2.1}$$

$$\frac{\partial\rho}{\partial t}+\nabla\cdot(\rho\mathbf{u})=0, \tag{2.2}$$

where,

ρ = density of the fluid,
$\mathbf{u}$ = flow velocity,
p = flow pressure,
$\boldsymbol{\tau}$ = stress tensor,
$\mathbf{f}$ = body forces.

The left side of equation 2.1 is an acceleration term in both time (mass acceleration) and spatial coordinates (advection of mass). The right hand side of the equation the hydrostatic forces, body forces and the divergence of deviatoric stresses.

In general the above equations can not be solved analytically, due to the non-linearity of the advective term. In cases where this non-linear term is dominant, the system gives rise to turbulence. Turbulence is the chaotic behaviour of the flow due to fluctuations of the velocity, pressure and other convective transferred quantities, in time and space. In engineering applications though we are more interested in mean values rather than the exact motion of the fluid. Models for predicting the mean velocity pressure and temperature distributions have been developed for turbulent flows. As an initial attempt to model a heat exchanger, we wanted to keep the problem simple, by ignoring the non-linear term.

In a steady state flow all the states of the system become time invariant, therefore the first term of equation 2.1, which is the time dependent acceleration term, becomes zero. Furthermore for incompressible flows the stress tensor $\boldsymbol{\tau}$ can be expressed according to Stokes constitutive equation for a Newtonian fluid, as follows:[14]

$$\boldsymbol{\tau} = \mu(\nabla\mathbf{u} + (\nabla\mathbf{u})^{\mathbf{T}}) \tag{2.3}$$

where, μ is the dynamic viscosity of the fluid. In cases where the mass advection is small compared to the rest of the terms, the non-linear part of equation 2.1 can be dropped. The resulted equation 2.4 describes a flow known as Creeping or Stokes flow:

$$\nabla p = \nu\nabla^2\mathbf{u} + \mathbf{f}, \tag{2.4}$$

$$\nabla\cdot\mathbf{u} = 0, \tag{2.5}$$

where, ν is the kinematic viscosity. In order to solve the above Partial Differential Equations (PDEs), the boundary conditions must also be known. Typical heat exchanger set-ups are modelled by assuming a fully developed flow at the entrance, which leads to a laminar velocity profile in combination with the previous assumptions. As a typical outlet we assume constant pressure.

Furthermore no-slip conditions are imposed at the solid boundaries, that enforces the fluid to have zero velocity. For the internal structures of the heat exchanger we will introduce an alternative to the standard method of imposing this no-slip condition, known as the Brinkman penalization method. This method of calculating flows around obstacles is used in problems where the geometry is complex. It is based on the Darcy law that describes flows in porous media [15]. By introducing a frictious force term in the momentum equation 2.4, we can model the solid state areas as highly dense porous regions:

$$\alpha(\mathbf{x})\mathbf{u} = -\nabla p + \nu\nabla^2\mathbf{u} + \mathbf{f}, \tag{2.6}$$

where,

α = inverse permeability, a spatial property of a porous media.

When α takes high values in a certain domain then that domain becomes relatively impermeable to the flow and the flow will be directed around. Likewise, when α is zero, the original Stokes flow equation is retrieved, presenting no obstacle, as explained in the table below:

Inverse Permeability (α)	Velocity (u)	Effect on the Flow
0	Governed by Stokes equation 2.4	Unobstructed flow
∞	0	Obstructed flow (solid structure)

2.2. HEAT TRANSFER

Heat transfer is the process of exchanging thermal energy by means of temperature changes. The main mechanisms for heat transfer are conduction, advection and radiation.

2.2.1. CONDUCTION

Conduction is a contact mechanism, which transfers energy at a rate proportional to the temperature difference. On the macroscopic level the convection heat transfer is governed by Fourier's Law: [16]

$$\mathbf{q} = -k\nabla T. \tag{2.7}$$

For systems that only exhibit heat conduction the above equation can be written in a conserved form of:

$$\nabla \cdot (\mathbf{q}) = 0 \implies -\nabla \cdot (k\nabla T) = 0, \tag{2.8}$$

where,

$$\begin{aligned}
\mathbf{q} &= \text{is the heat flux density,}\\
k &= \text{is the material conductivity,}\\
T &= \text{is the temperature field.}
\end{aligned}$$

In the general case of an anisotropic material (properties of the material are direction dependent), the conductivity is a second order tensor and represents how well a material conducts the heat. Other than the direction, conductivity can also be spatial and temperature dependent. In this study we considered isotropic, uniform and temperature invariant materials. As a result the conductivity becomes a scalar location dependent property.

Typical boundary conditions for a conductive problem are a prescribed temperature $T_S = T_o$, thermal insulation or zero heat flux $\nabla T \cdot \mathbf{n} = 0$, heat convection $\nabla T \cdot \mathbf{n} = h(T_S - T_{ext})$, boundary heat source $q_S = q_o$, and radiaton $\nabla T \cdot \mathbf{n} = \epsilon\sigma(T_{ext}^4 - T_S^4)$.

2.2.2. ADVECTION

Advection is the transportation of heat due to the fluid motion. Therefore this mechanism of heat transfer is only present in problems where the medium is moving. The advection equation for a conserved quantity ψ of a velocity field $\mathbf{u}$ is: [16]

$$\frac{\partial \psi}{\partial t} + \nabla \cdot (\psi \mathbf{u}) = 0. \tag{2.9}$$

In the case of an incompressible flow, where $\nabla u = 0$, equation 2.9 becomes:

$$\frac{\partial \psi}{\partial t} + \mathbf{u} \cdot \nabla \psi = 0. \tag{2.10}$$

If we consider ψ to be the specific enthalpy h, and considering that $dh = \rho c_p dT$ then equation 2.10 becomes:

$$\rho c_p (\frac{\partial T}{\partial t} + \mathbf{u} \cdot \nabla T) = 0, \tag{2.11}$$

where,

ρ = density of the fluid,
c_p = heat capacity at constant pressure,
T = Temperature,
$\mathbf{u}$ = flow velocity.

The same boundary conditions found in conductive problems can also be applied in advective problems.

2.2.3. THERMAL RADIATION

With the term thermal radiation we refer to the electromagnetic radiation emitted by any body due to temperature. Any body with temperature above the absolute zero emits thermal radiation and it differs from the two previous transfer mechanisms from the fact that there is no need for a medium. Stefan-Boltzmann law describes the power radiated per unit surface area p by a black body of temperature T: [16]

$$q = \epsilon\sigma T^4 \tag{2.12}$$

where,

ϵ = the emissivity of the body,
σ = the Stefan–Boltzmann constant.

As seen in the above equation the heat transfer due to radiation scales to the fourth order of the temperature. This means that for relatively high temperatures radiation becomes dominant. In typical applications of heat exchangers with low temperature flows, thermal radiation can be neglected in favour of conductive or advective heat transfer. In this study we did not study cases where heat is transferred by thermal radiation, but there is no limitation in including the effects of thermal radiation.

2.3. HEAT TRANSFER IN HEAT EXCHANGERS

In this study we are interested in heat exchangers without a phase change. This means that the main mechanism of heat transfer is convection (advection and conduction). Such a system can be described by the following equation:

$$\rho c_p(\frac{\partial T}{\partial t} + \mathbf{u}\cdot\nabla T) + f_t - \nabla\cdot(k\nabla T) = 0, \tag{2.13}$$

where,

f_t = heat generation (due to heat source, viscous dissipation etc.)

The first term of the left hand side of 2.13 corresponds to the advective term, while the right hand side corresponds to the conductive term. The heat transfer problem is coupled with the flow problem, since equation 2.13 is dependent on the unknown velocity vector field. In the case of isothermal flow the problem becomes one way coupled. This means that the flow problem can be solved separately from the heat transfer problem. The typical boundary conditions used in conductive and convective problems, can also be applied in heat exchangers.

2.4. DIMENSIONLESS ANALYSIS

In order to be able to quantify the phenomena and physical quantities happening in a flow or a heat transfer problem, and disjoint them from case dependent dimensions, dimensionless analysis is introduced. The following dimensionless quantities are important in describing a heat exchanger problem: [17]

Peclet number $P_L = \frac{\text{advective heat transfer}}{\text{condutive heat trasfer}} = \frac{\mathbf{u}L}{a} = Re_L Pr.$
Where L is the characteristic length, u is the velocity and $a = \frac{k}{\rho c_p}$ is the thermal diffusivity. In common applications this number is greater than unity which means that the main driving mechanism of heat transfer is advection.

Reynolds number $Re = \frac{\text{inertial forces}}{\text{viscous forces}} = \frac{\mathbf{u}L}{\mu}.$
Where L is the characteristic Length, u is the relative mean velocity of the fluid and v is the kinematic viscosity. A low Reynolds number indicates a laminar flow, since the inertial forces are not significant relative to the viscous forces. A flow characterised by a Reynolds number lower than the unity can be sufficiently described by the Stokes equations.

Prandtl number $Pr = \frac{\text{viscous diffusion rate}}{\text{thermal diffusion rate}} = \frac{v}{a}.$
Where v is the kinematic viscosity and $a = k/(\rho c_p)$ is the thermal diffusivity. A problem described by a high Prandtl number indicates that the thermal boundary layer propagates faster than the velocity layer. Since Prandtl and Peclet, and Reynolds numbers are related, one can choose two of them to describe a problem.

Nusselt number $Nu_L = \frac{\text{Convective heat transfer}}{\text{condutive heat trasfer}} = \frac{Lh}{k}.$
Where h is the thermal convection coefficient, k is the conductivity and L is the characteristic length. Nusselt number is typically a function of the other dimensionless numbers described above and empirical formulas exist for many common flow problems. In cases of non standard geometries, such as the designs we aim to produce with topology optimization, it is impossible to find any relative correlation of the Nusselt number.

From now on the problems will be described in terms of dimensionless numbers.

3
Topology optimization

In this chapter we discuss the basic concepts of topology optimization, we review the relative work of topology optimization problems, and based on that, we make a first attempt to optimize a heat exchanger. Topology optimization as explained in Bendsoe's work [8] is a "material distribution method for finding the optimum lay-out structure" of a problem. The lay-out refers to both the shape and material of a structure. What separates topology optimization from the other structural optimization methods is that the optimization variables concern the whole design space, instead of specific characteristics of the design. A simple example of topologically optimizing a heat exchanger, would be to find the optimal shape of the channels for maximum heat transfer (see figure 3.1).

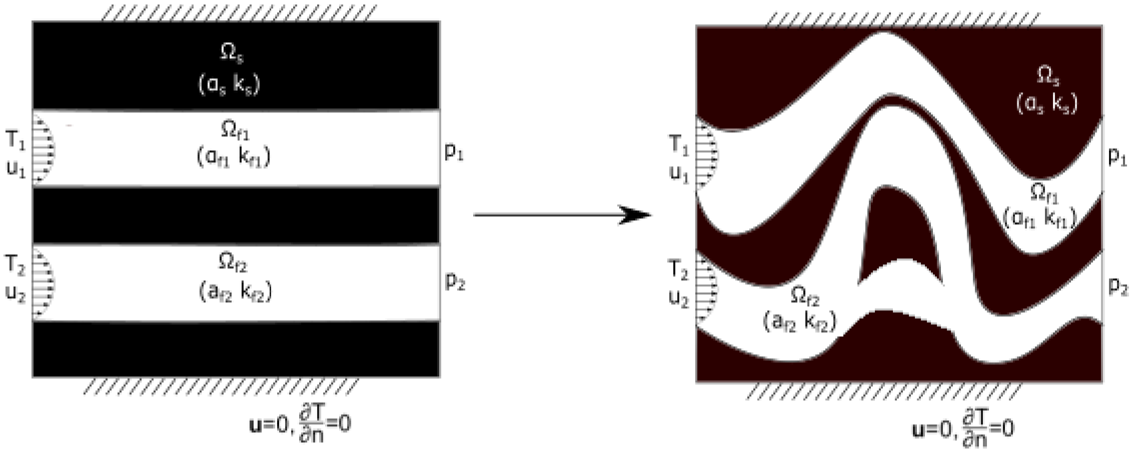

Figure 3.1: An example of topology optimization process from a naive to a non trivial optimised design.

The problem can be mathematically formulated as shown below:

$$
\begin{aligned}
&\underset{\boldsymbol{\gamma}}{\arg\max/\min} H(\boldsymbol{\gamma},\mathbf{u}(\boldsymbol{\gamma})),\\
&\quad\text{subject to:}\\
&\qquad\qquad \text{governing equations,}\\
&\qquad\qquad \text{boundary conditions,}\\
&\qquad\qquad g_i(\mathbf{u},\boldsymbol{\gamma}) = 0,\ i = 1,\dots,n,\\
&\qquad\qquad h_j(\mathbf{u},\boldsymbol{\gamma}) \le 0,\ j = 1,\dots,m,\\
&\qquad\qquad \boldsymbol{\gamma}_k^{\min} \le \boldsymbol{\gamma}_k \le \boldsymbol{\gamma}_k^{\max},\ k = 1,\dots,l,
\end{aligned}
\tag{3.1}
$$

where,

(a) Discretised design domain. Each square can be either solid or fluid.

(b) Design that illustrates a random topology of the solid and fluid material. Black and white regions represent solid and fluid domains respectively.

Figure 3.2: Discrete property of the design variable of a topology optimization problem. [18].

H = the objective function that we want to maximize/minimize,
$\boldsymbol{\gamma}$ = the design variables,
$\mathbf{u}$ = the state variables,
g_i = equality constraints,
h_j = inequality constraints,

The objective function H, quantifies the performance of the system, e.g. the transferred heat (from the hot to the cold fluid), and in general can be a function of both the state and the design variables. In physical processes the state variables are dictated by the governing equations of the system. In most cases those governing equations can be linearised and discretised to a system of linear algebraic equations in the form of $\mathbf{K}(\boldsymbol{\gamma})\mathbf{u}(\boldsymbol{\gamma}) = \mathbf{b}$. Furthermore physical limitations, or performance requirements dictate the inequality (g_i) and equality constraints (h_j). Equation 3.1 describes any general optimization problem. What defines a topology optimization problems is the choice of the design variables.

In topology optimization we are interested in finding where the material should be positioned. This can be quantified by assuming a space dependent state property $\gamma_n\mathbf{x}$. In an optimization problem where only two states are possible, $gamma$ becomes:

$$\gamma_n(\mathbf{x}) = \begin{cases} 0 & \text{if } \mathbf{x}_n \text{ is in state 1} \\ 1 & \text{if } \mathbf{x}_n \text{ is in state 2} \end{cases}.$$

In figure 3.2 an example of a discrete design variable of a flow problem is shown. The design variable can obtain one of the two states; solid or fluid, which are visualised as black and white regions, respectively.

The example in figure 3.2 although small in size has 2^{16} unique combinations. A common approach to solve the discrete value problem is to change the discrete variables to continuous ones, (see Bendsoe et al. [8]). The transformation of the problem from a discrete to a continuous one, allows us to use optimization algorithms that make use of derivatives in order to find the extrema, a process that will be referred from now on as sensitivity analysis. A brief explanation of the sensitivity analysis is given in appendix B. In the next section we discuss how topology optimization has been successfully applied to problems related to heat exchangers.

3.1. LITERATURE REVIEW OF TOPOLOGY OPTIMIZATION PROBLEMS

A heat exchanger is governed by multi-physical phenomena. In order to model a heat exchanger, one has to solve both the flow and the heat transfer problem. Therefore, we review cases where topology optimization has been applied to flow and heat transfer problems.

3.1.1. CONDUCTIVE HEAT TRANSFER PROBLEMS

Topology optimizations has been used in various applications related to heat transfer problems. One relatively simple problem in the heat transfer category is of a solid heat sink. These devices are used to efficiently cool an area of interest.

G.Marck et al. of [19] studied the conductive problem of cooling an electronic device. The problem is defined as minimizing the temperature over a uniformly heated domain, in addition to keeping a uniform temperature distribution over the domain. The amount of highly conductive solid material available is limited, prohibiting full solid designs. These multi-objective optimization problems are used when there more than one quantities of interest. Each objective contribution is weighted to the total objective. Assigning proper weights is not always easy as one must have good understanding of the behaviour of the objectives.

Similar works can be found on purely conductive problems that show the same root like solid structures, in the studies of Gao et al. [20], Li et al. [21], Xie et al. [22], Zhuang et al. [23].All these problems work on different design domains and boundary conditions, but they have similar objectives, relating to te cooling of the device.

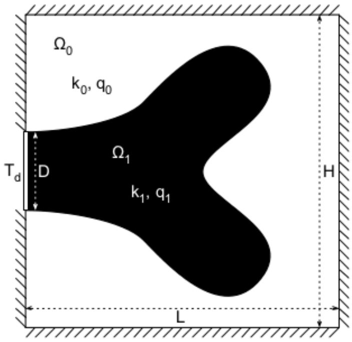

(a) Design domain and boundary conditions of the problem. Initial design.

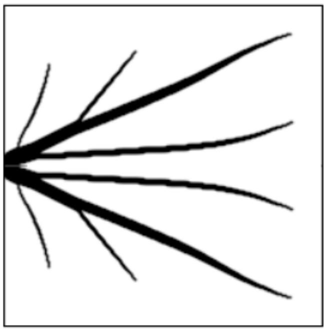

(b) Optimal design.

Figure 3.3: a) design domain and an initial suboptimal design b)optimal topology of the sink heat[19]. Black and white coloured regions, are areas of highly and lowly conductive material respectively

3.1.2. FLOW PROBLEMS

Another category of problems related to heat exchangers, where topology optimization has been applied, are laminar flow problems. The main goal of such problems is the minimization of the pressure drop along the flow. In the work of [24] the problem of minimizing the pressure drop through a channel is studied (see figure 3.4). They define the cost function of energy loss due to viscosity as:

$$\Phi = \frac{1}{2}\int_{\Omega} [\nabla \mathbf{u}(\nabla \mathbf{u} + (\nabla \mathbf{u})^T) + \alpha \cdot \mathbf{u} \cdot \mathbf{u}^{\mathbf{T}}]\, d\Omega.$$

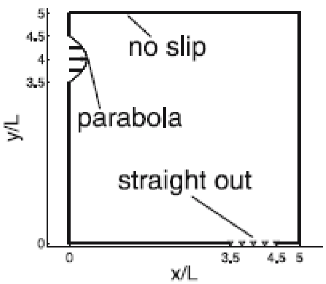

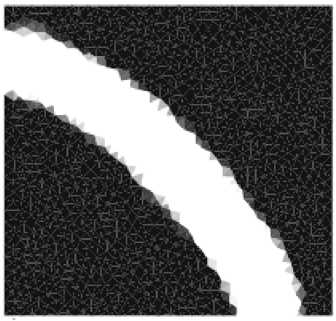

Figure 3.4: Design domain and optimal channel topology of minimal pressure drop [24]. Black and white regions are solid and fluid areas respectively.

A similar problem but with different approach on the objective function, was done in the work of Marck et al. [11], where the energy loss is calculated over the boundaries. More examples of topology optimization applied to flow problems can be found in the work of Borval et al. [12], Guest et al. [25], Olesen et al. [26].

Figure 3.5: Optimised design for varied pressure drop[10]. The black regions are regions of highly conductive solid material, and the white regions of fluid material. The fluid enters the system from the top boundary and exits from the bottom one. Heat is generated throughout the domain.

3.1.3. CONVECTIVE HEAT TRANSFER PROBLEMS

A step closer to multi-flow heat exchangers are the convective heat transfer problems, that include both mass and heat transfer. The common aspect of these problems is that a domain is heated and the objective is to cool it up by using a fluid as a coolant medium.

LAMINAR FLOW PROBLEMS

There is a lot of research done in topology optimization in heat transfer of laminar flows. In the work of Marck et al. [11] a convective cooling problem is studied. A multi objective function is used at the boundaries of the system, to include both the maximization of the transferred thermal energy by the fluid, and the minimization of the pressure drop. A similar approach has been used in this thesis, modified for the needs of a heat exchanger, as it will be explained in later in the chapter. Similar studies can be found for laminar flow cooling devices, working on different geometries, boundary conditions, and objective functions.

In the work of Koga et al. [10] a sink is optimized for minimizing the temperature of the domain. The objective function used for maximizing the heat transferred out of the system is formulated as:

$$\Phi = \frac{1}{2}\int_{\Omega} k\nabla \cdot T\nabla T + \rho c_p(\mathbf{u}\cdot\nabla T)\, d\Omega - \int_{\Omega} qT\, d\Omega. \tag{3.2}$$

As the paper explains "The first term 3.2 aims for the maximization of the heat transfer, where the temperature is fixed, and the second term aims for the minimization of the temperature, when a heat source is applied. Although the first term seems promising for a heat exchanger optimization problem, in reality it only works for problems with heat generation. The term becomes zero when there is no heat source and therefore is independent of the design.

A similar study to [10] was done by M.Dede [27] for flows of a low Reynolds number. The resulted optimal solution illustrated root like structures, similar to the optimised solutions of the conductive heat problems (see figure 3.6). In the work of Alexandersen [9] buoyancy is also taken into account, in the problem of optimizing a natural and forced convection cooled heat sink.

TURBULENT FLOW PROBLEMS

Not much research has been done for turbulent flow problems in ducted flows, due to the complexity of the phenomena. A characteristic work is of Papoutsis et al. [28], where turbulent heat transfer problems are studied using Spalart-Allmaras turbulence model (see [29]). This work showed that the optimizing of turbulent duct flows is possible.

Figure 3.6: Optimised design showing root like structure[27]. The black regions are regions of highly conductive solid material, and the white regions of fluid material. The fluid enters the system from the left boundary and exits from the right one. Heat is generated throughout the domain.

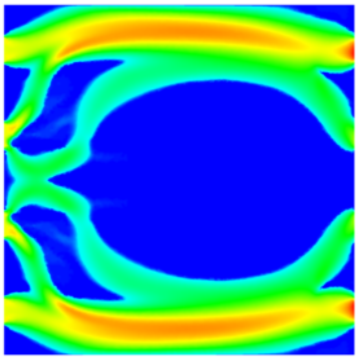

Figure 3.7: Velocity field of the optimized design of a turbulent flow heat sink[28].

3.2. TOPOLOGY OPTIMIZATION OF HEAT EXCHANGERS

In this section we will define a procedure to optimize the topology of a heat exchanger. In order to find an optimal design the problem must be set in the form of 3.1. The quantity of interest for optimization is set to be the maximization of the heat transfer. Together with minimization of the pressure drop are the most important aspects of heat exchangers as they translate into better efficiency and reduced operating costs. We avoided using a multi-objective function that includes both the maximization of the heat transfer and pressure drop, as it would require a fine tuning of the objectives. This is due to the objectives not behaving in a similar manner to the changes of the topology. For example reducing the width of the channels to half may increase the pressure drop by a factor of 8, but only increase the heat transfer by a factor of 2. This would mean that the minimization of the pressure drop objective would dominate over the maximization of the heat transfer. Furthermore even if the objectives are properly adjusted, it is not easy to distinguish their contribution to the objective, which provides little insight on the optimized designs. Therefore we chose to only maximize the heat transfer:

$$\underset{\boldsymbol{\gamma}}{\arg\max/\min} \quad H = \int_{\Omega} \dot{q}_{\text{if}}\, d\Omega, \tag{3.3}$$

The energy conservation equation for just one fluid is:

$$\dot{q}_{\text{in}} + \dot{q}_{\text{if}} = \dot{q}_{\text{out}} - \dot{q}_{\text{g}}. \tag{3.4}$$

where,

$\dot{q}_{\text{if}}$ = the power transferred due to heat transfer between the two fluids through their interface,
$\dot{q}_{\text{in}}$ = the power getting in the system through the rest of the boundaries,
$\dot{q}_{\text{out}}$ = the power getting out the system through the rest of the boundaries,
$\dot{q}_{\text{g}}$ = the power generated over the domain.

We assume that the system is thermally insulated, so the only energy that comes into the systems is from the enthalpy influx due to the enthalpy carried by the fluid. Furthermore there is no heat generation, so equation 3.4 is equivalent to:

$$\dot{q}_{\text{if}} = \dot{q}_{\text{out}} - \dot{q}_{\text{in}} = \mathbf{u}_{\text{out}} c_p T_{\text{out}} - \mathbf{u}_{\text{in}} c_p T_{\text{in}}. \tag{3.5}$$

The properties of the fluid are assumed to be invariant of temperature, so equation 3.3 is equivalent to:

$$\underset{\gamma}{\arg\max/\min} \quad H = \int_{\text{outlet}} T_{\text{out}} \mathbf{u}_{\text{out}} \cdot \mathbf{n} \, dA. \tag{3.6}$$

Although we do not include the pressure drop in the objective function, we prescribe a maximum pressure at the two inlets (equation 3.7). The pressure is associated with the pressure drop and subsequently the power requirements.

$$\int_{\text{inlets}} p \, dA \leq p_o. \tag{3.7}$$

When optimizing the topology of a heat exchanger, we are interested to find where the solid material will be placed and subsequently where the fluid will flow. Therefore, the two states of the design variable become the solid and the fluid state. What distinguishes the solid from the fluid states are the properties of the materials. Looking at the governing equations for the flow (equation 2.6) and the heat transfer equation 2.13, the state properties that describe the material are:

α = the permeability,
ρ = the density,
c_p = the specific heat capacity under constant pressure,
k = the conductivity.

In equation 2.13, ρ and c_p are multiplied by the velocity field, which becomes zero in the solid regions. Therefore the value of these properties in the solid state is not important. Choosing c_p and ρ to have the same value over the two states simplifies the problem. The remaining properties, $\alpha(\gamma)$ and $k(\gamma)$, become a function of the design variable γ in a way that the solid and fluid states are correctly represented:

$$\gamma(\mathbf{x}) = \begin{cases} 0 & \text{if } \mathbf{x} \text{ is fluid} \\ 1 & \text{if } \mathbf{x} \text{ is solid} \end{cases},$$

and,

$$\begin{aligned} \alpha(\gamma = 0) &= 0, & \alpha(\gamma = 1) &= \infty, \\ k(\gamma = 0) &= k_f, & k(\gamma = 1) &= k_s. \end{aligned} \tag{3.8}$$

Where, k_f and k_s are the conductivity of the fluid and solid states respectively. We interpolate those limit values, in order to transform the problem from discrete to a continuous one, by assigning intermediate values to the properties, using a continuous RAMP function [30].

The maximization problem is subjected to the governing equations of the steady state problem. As a starting point and due to simplicity we decided to investigate low Reynolds number flows governed by equation 2.6. Assuming no body forces (eg. gravitational) equation 2.6 is equivalent to equation 3.9, and together with the conservation of the mass 2.5 constitute the governing equations of the flow problem. Similarly the heat transfer equation 2.13 in the steady state is equivalent to equation 3.10.

$$\alpha(\gamma)\mathbf{u} = -\nabla p + \mu \nabla^2 \mathbf{u}, \tag{3.9}$$

$$\rho c_p \mathbf{u} \cdot \nabla T - \nabla \cdot (k(\gamma) \nabla T) = 0. \tag{3.10}$$

Furthermore the design variable γ is bounded to the [0,1] space:

$$0 \leq \gamma \leq 1 \tag{3.11}$$

Equations 2.5, 3.6, 3.7, 3.9, 3.10 and3.11 constitute the optimization problem:

$$\begin{aligned}
&\underset{\boldsymbol{\gamma}}{\arg\max/\min} H = \int_{\text{outlet}} T_{\text{out}} \mathbf{u}_{\text{out}} \cdot \mathbf{n}\, dA, \\
&\text{subject to:} \\
&\qquad \rho c_p \left(\frac{\partial T}{\partial t} + \mathbf{u} \cdot \nabla T\right) + f_t - \nabla \cdot (k \nabla T) = 0, \\
&\qquad \alpha \mathbf{u} = -\nabla p + \mu \nabla^2 \mathbf{u} + \mathbf{f}, \\
&\qquad \nabla \cdot \mathbf{u} = 0, \\
&\qquad \mathbf{u}_S = \mathbf{0}, \\
&\qquad \mathbf{u}_{\text{inlet}} = \mathbf{u}_{\text{lam}}, \\
&\qquad p_{\text{oultet}} = p_{\text{ext}}, \\
&\qquad T_{\text{inlet}} = T_{\text{in}}, \\
&\qquad \nabla T_S \cdot \mathbf{n} = 0, \\
&\qquad \nabla T_{\text{oultet}} \cdot \mathbf{n} = 0, \\
&\qquad \int_{\text{inlets}} p\, dA \leq p_o. \\
&\qquad 0 \leq \boldsymbol{\gamma}_k \leq 1,\ k = 1, \ldots, l,
\end{aligned} \tag{3.12}$$

where,

H	= the objective function that we want to maximize/minimize,
$\boldsymbol{\gamma}$	= the design variables,
$\mathbf{u}_{\text{lam}}$	= laminar parabolic profile,
p_{ext}	= external pressure,
inlet, outlet, S	= inlets, outlets, and the rest external boundaries respectively.

3.3. A FIRST APPROACH

In this chapter we will make first approach to solve the optimization problem of a heat exchanger, as formulated in equations 3.6, 3.7 and 3.11 in section 3.2. We simplify the problem to two dimensions by assuming an infinitely deep design. Although in practice 2D heat exchangers do not exist, they are simpler to model, and computationally less expensive to solve, since they require less time and memory. Working in 2D although highly advantageous, poses some realistic limitations for the designs. One limitation is that the two flows hold the same position relative to each other, which means that one flow will always be on the same side of the other. Because of that, the heat is transferred from one fluid to the other always in the same direction. Furthermore there can be no vorticity parallel to the velocity field, allowing for a circulation of the temperature layers. Nevertheless the simplification of the problem will give us a better understanding of the resulted designs.

The design domain is a square, with two inlets and outlets, as shown in figure 3.8. The boundary conditions were taken as follows.

1. Prescribed parabolic velocity profile at the inlets.
2. Prescribed constant temperature at the inlets.
3. Prescribed pressure at the inlets without backflow.
4. No slip condition and zero thermal flux on the boundaries.

The characteristic Reynolds number of the flow problem is 0.02, based on the average velocity at the inlets and the length of the domain, which is well below the limit of Stokes flow regime that we use. We use a high Peclet number of 20 which means that the main means of heat transfer is convection. We choose such

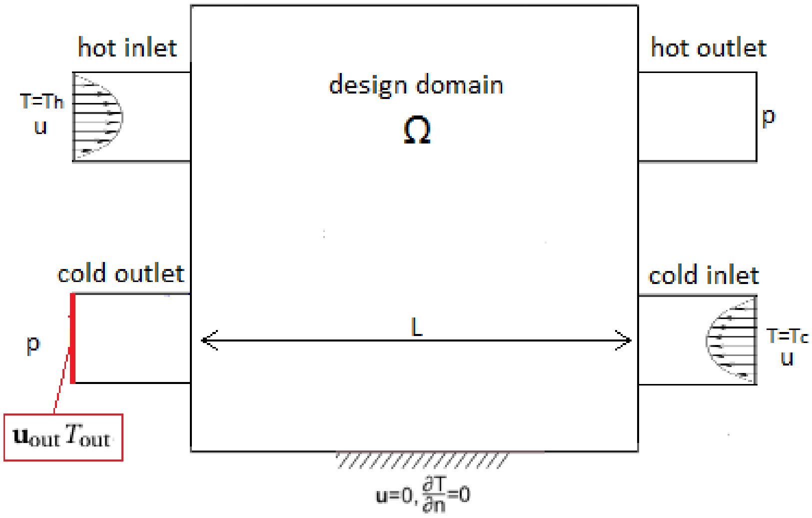

Figure 3.8: A 2D heat exchanger. The central square domain is the design domain Ω. The inlets and outlets are not part of the design space. The characteristic length L used to calculate the Reynolds, Prandtl, and Peclet number is the length of the design domain. The objective function calculated at the bottom right outlet is shown in red colour. The boundary conditions for the heat transfer and flow problems can be seen.

a large Peclet number, so that the theoretical maximum efficiency can not be achieved by a trivial design. Doing otherwise would produce designs, where the temperature of the two fluids come into equilibrium, even in simple designs (see section 5.2.1), making the optimization process obsolete. The allowed pressure at both the inlets is set to be 6 times higher than it would be in a fully open design, to allow for complex channel designs, of high length and reduced width. One way of maximizing the heat transfer, is by increasing the effective surface area between the two flows. Another one is by reducing the width of the channel, thus reducing length the temperature profile. Having these in mind one would expect the design to have as long and narrow channels as possible. The resulted optimized design, shown in figure 3.9, did not have any of the above characteristics.

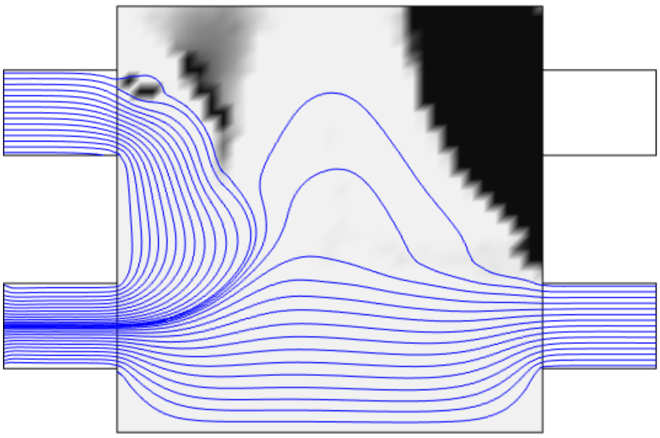

Figure 3.9: Optimized short circuit design. The stream lines (blue lines) coming from the two inlets, both exit from the cold outlet. The black regions represent the solid material placement. The hot outlet is actively blocked by a solid wall.

3.3.1. ANALYSIS OF THE RESULT

The resulting topology is a design where both flows exit from the same outlet creating a short circuit design. The outlet on the top right corner that was intended for the hot flow is now blocked by impermeable material (black coloured area), forcing both flows to exit from the outlet intended for the cold flow. This maximizes the enthalpy of the flow that exits from the outlet, since all of the enthalpy of the system exits from there. However it does not maximize the heat transfer between the two flows. This is due to the fact that we assumed that only one fluid exited from the cold outlet (see assumptions of equation 3.4), which is not the case for this design. In order for the assumption to be valid the inlets must be connected uniquely to the outlets. An example of such a configuration can be seen in figure 3.10, where both flows exit from their corresponding outlet. in this case although less total energy exits from the cold outlet, the heat transfer is higher due to a longer interface length.

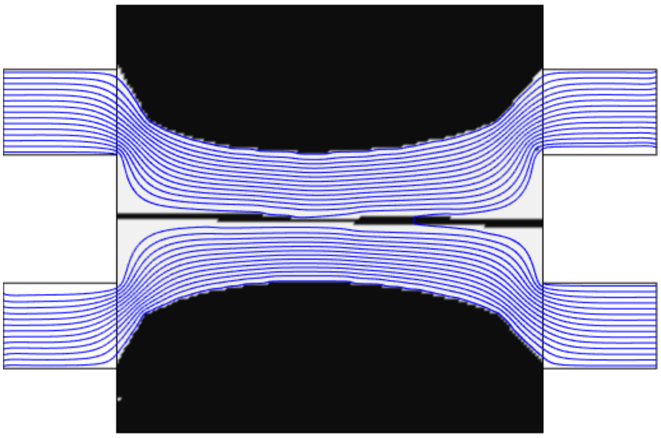

Figure 3.10: Typical heat exchanger that is not short circuited. The two flows exit from unique outlets. Heat is transferred from the hot to the cold fluid through the interface of the two flows.

Changing the objective to the minimization of the enthalpy coming out of the hot outlet, results in a similar design, as it is not possible for the optimizer to distinguish which outlet corresponds to which inlet (see figure 3.11).

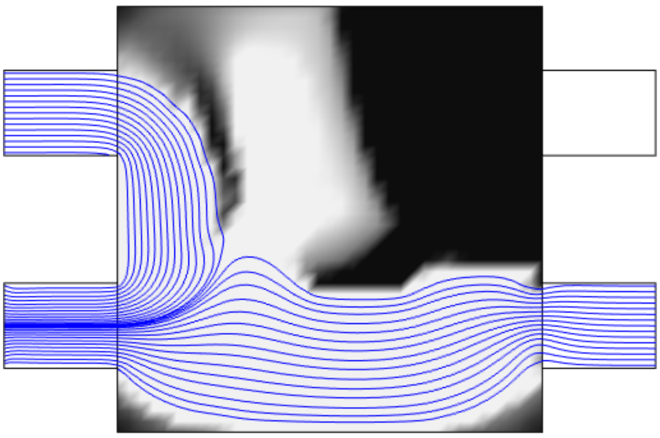

Figure 3.11: Changing the objective function to minimizing the enthalpy flux from the hot outlet results in a similar design.

In order to be able to produce a correct design for a heat exchanger, we need to find a way to solve the short circuit problem. In addition to that we need to find a way to separate the two flows, so no mixing of the two flows happen.

4

Fluid Tracking Model

One way of restricting the flows to the predefined outlets is by tracking them and forcing them to exit from the correct outlet, by penalising any short-circuit behaviour. With the term tracking we mean to be able to identify from which inlet does the fluid of a specific region originated from. Many tracking methods exist in identifying and tracking the interface of multiphase flows. A popular method for such problems, is the Level Set Method (see Chang et al. [31] for more details), which is used for tracking the moving interface of a multiphase flow. this is done by solving an extra set of transport equations and finding the zero level of a transported quantity that describes the interface:

$$\mathbf{u} \cdot \nabla \psi = \frac{\partial \psi}{\partial t}. \tag{4.1}$$

Many more methods exist, such as the Phase Field Model (see Jacqmin [32]), or the Euler-Euler Model (see Fedkiw et al. [33]), but we did not have time to investigate all of them.

We implemented a variant of the level set method 4.1 used in multiphase flow problems, that we modified for stationary problems, as shown in equation 4.2. We introduced a temperature-like quantity "ψ" that is transported by advection. A value of ψ is assigned at every inlet, which gets tracked across the domain. The method can be easily visualised as putting a dye of different colour at each inlet.

$$\mathbf{u} \cdot \nabla \psi = \nabla \cdot (k_\psi \nabla \psi). \tag{4.2}$$

The left hand side of equation 4.2 is the advection of ψ by the velocity field. The right hand side is a diffusion term required for stabilised solutions. In order to get stable solutions, the Peclet cell number should be less than a certain value [34].

The boundary conditions are set in a similar manner to a heat transfer problem. There is a prescribed constant value of ψ at the inlets and zero influx ($\mathbf{n}\nabla\psi = 0$) at the rest of the boundaries. More specifically we set ψ to be -1 at the hot inlet, and 1 at the cold one. Then we proceed in solving equation 4.2 by using the velocity solution of the flow problem.

We solved the tracking problem for the design shown in figure 4.1a of an open domain. Figure 4.1b shows how ψ is conserved across the flow, making it easy to track the region of the flow that originated from the cold inlet. The areas between the two flows get intermediate values, and the width of this area is dependent on the diffusion coefficient and the mesh size.

The same problem was solved for the case where a solid wall is separating the two flows (see fig 4.2a). The velocity at the solid region approaches zero, making diffusion the dominant term. In figure 4.2b can be seen how ψ diffuses along the wall, resulting in intermediate values.

.

Although the value of ψ does not conserve in low velocity areas, this method seems promising as it makes it possible to distinguish between the two flows.

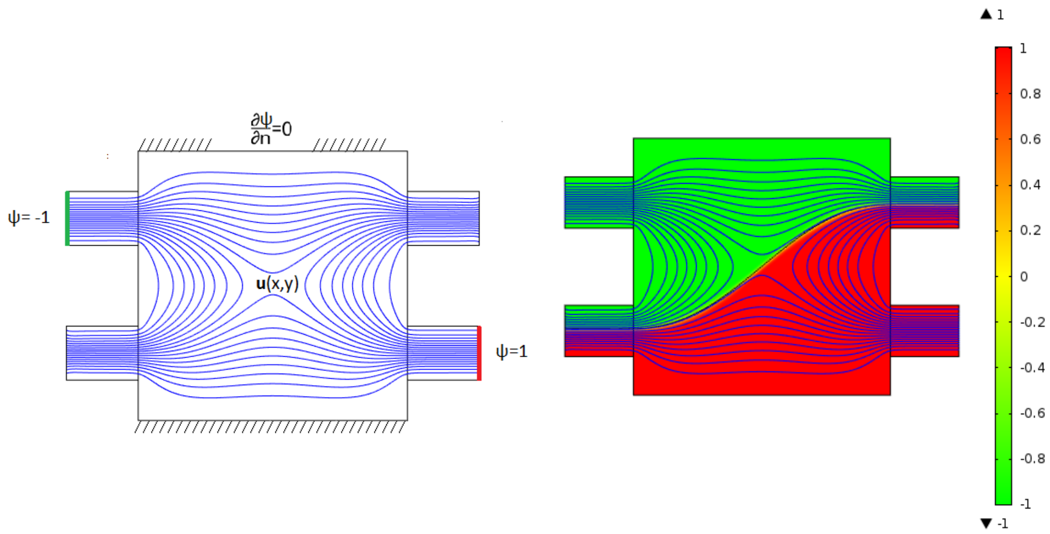

(a) Stream lines of an empty domain.

(b) ψ field of the two flows of an empty domain. The quantity is conserved along the domain.

Figure 4.1: Solution of the flow and tracking problem of a two inlet and outlet problem.

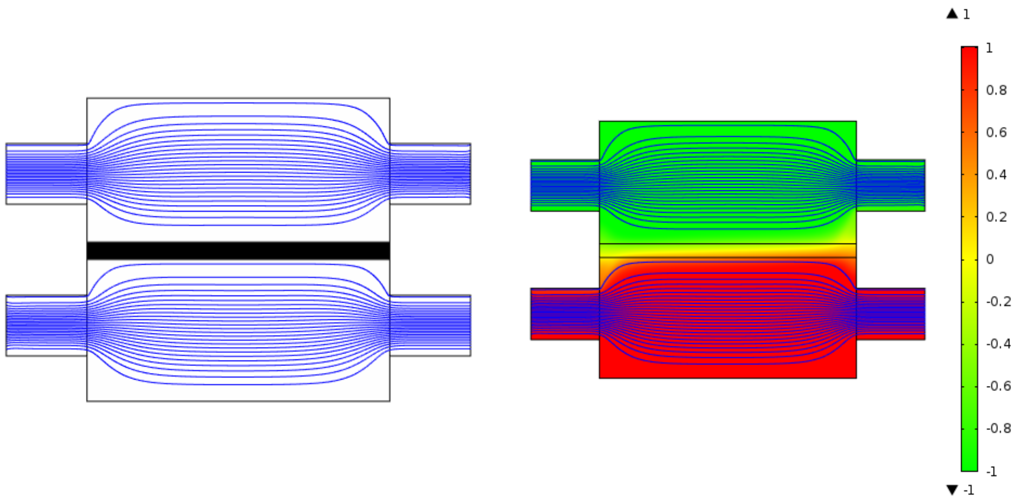

(a) Stream lines of the flows. The velocity in regions close to the wall approaches zero.

(b) ψ field of flows separated by wall. The quantity is no longer conserved along the domain.

Figure 4.2: Solution of the flow and tracking problem when the two flows are separated by a solid intermediate.

4.1. IMPLEMENTATION

In this section the tracking method will be implemented to the topology optimization model for heat exchangers, that was explained in section 3.3. Although ψ is not constant in areas of low velocity, we can still distinguish the flow regions by identifying two regions: one where $\psi < 0$, and one where $\psi > 0$:

$$\text{fluid originated from} \begin{cases} \text{first inlet} & \text{if } \psi(x, y) < 0, \\ \text{second inlet} & \text{if } \psi(x, y) > 0. \end{cases}$$

We do that by filtering ψ by an approximate continuous heaviside function, $\theta(\psi)$ (see figure 4.3):

$$\theta(\psi) \approx \begin{cases} -1 & \text{if } \psi(x,y) < 0, \\ 1 & \text{if } \psi(x,y) > 0. \end{cases}$$

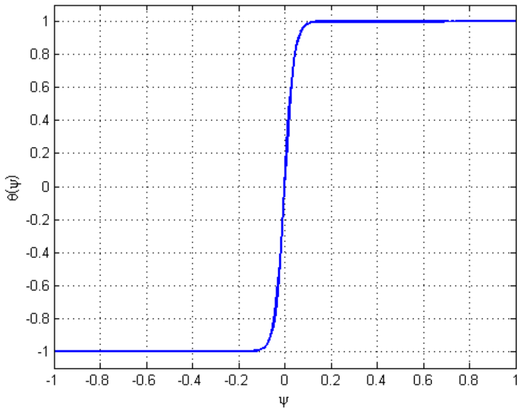

Figure 4.3: Approximate continuous heaviside function θ.

The objective function 3.6 can know be written as follows:

$$H = \int_{\text{outlet}} \theta(\psi)\, T\, \mathbf{u} \cdot \mathbf{n}\, dx. \tag{4.3}$$

This new objective penalises the hot fluid that exits from the cold outlet, making short circuits unattractive solutions for the optimizer. We can now define a procedure for the topology optimization problem as follows:

1. The flow problem is solved, and the velocity field is obtained (see figure 4.4).

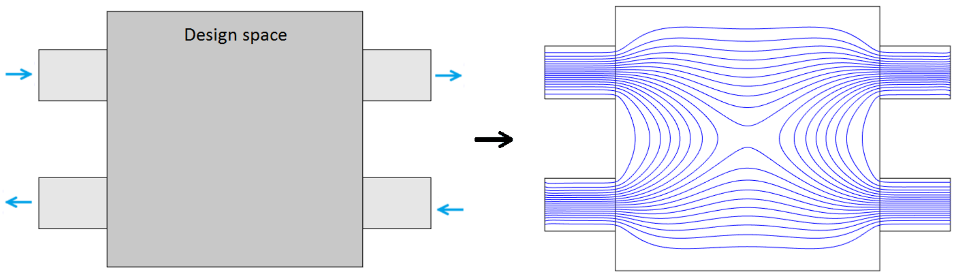

Figure 4.4: Flow problem and the solution. Stream lines of the flow.

2. For the given velocity field the tracking problem is solved (see figure 4.5).

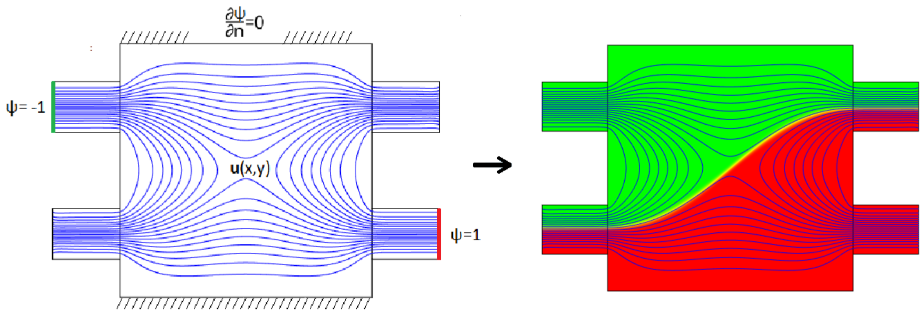

Figure 4.5: Tracking problem, and the resulted ψ field. The colours are associated with the inlet a specific fluid region originated from.

1. In parallel with the tracking problem, the heat transfer problem is solved (see figure 4.6).

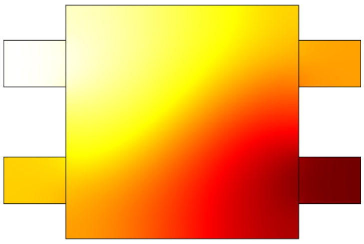

Figure 4.6: Temperature field acquired from solving the heat transfer problem.

2. The optimizer updates the design variables according to the sensitivity analysis that has been performed, so that the objective function 4.3 is maximized.

4.2. RESULTS

In this section we test the Fluid Tracking Model in the problem of section 3.3. We use two different initial designs: one where the design variable is $\gamma = 0.5$ over the domain (see figure 4.7), and the one where γ creates a wall separating the two flows (see figure 4.9).

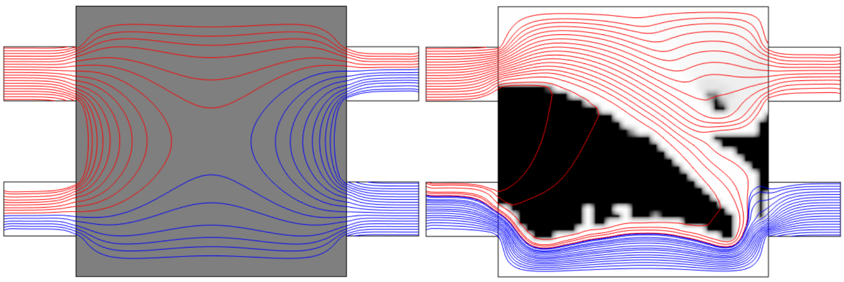

(a) Initial design. Design variable $\gamma = 0.5$ uniformly over the domain.

(b) Optimised design. Most of the hot flow exits from the cold outlet, but a small portion of it exits from the cold outlet.

Figure 4.7: Solution of the Fluid Tracking Method on a 2D heat exchanger of an initially semi-permeable design. The red and blue lines are stream lines for the hot and cold fluid respectively.

We can see in figure 4.7b that the optimized result does not completely solve the short-circuit problem. Although most of the hot flow is exiting from the hot outlet, a portions of it exits from the cold outlet. The optimization process seems to exploit the diffusion mechanism, by creating semi-permeable structures that allow the hot fluid to leak to the cold outlet, while diffusing the ψ quantity to a positive value.

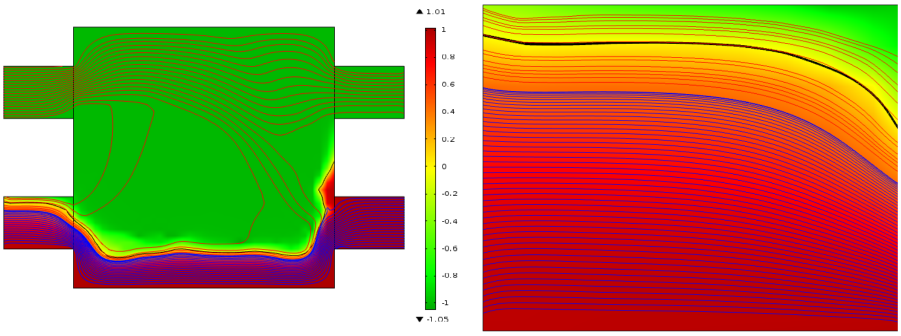

(a) Ψ field of the final solution. Ψ value of the hot fluid diffuses gradually from -1 to a positive value.

(b) Zoom into the cold outlet. The ψ value of the fluid that originated from the hot changes from -1 to a positive value.

Figure 4.8: Ψ field of the final solution along the design domain. The red and blue lines are stream lines for the hot and cold fluid respectively. The black line is the zero level contour of the ψ field.

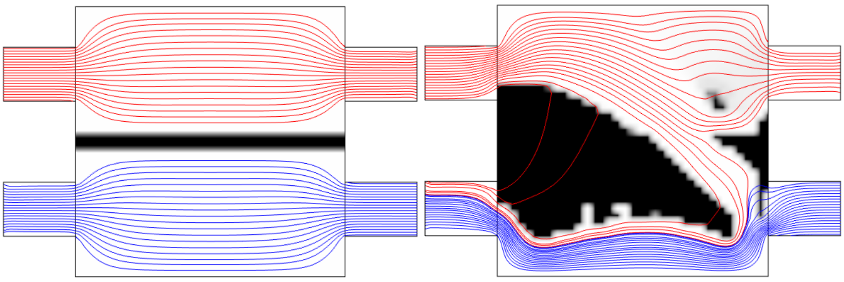

(a) Initial design. Design variable γ creates a wall that separates the two flows.

(b) Optimised design. Most of the hot flow exits from the cold outlet, but a small portion of it exits from the cold outlet.

Figure 4.9: Solution of the Fluid Tracking Method on a 2D heat exchanger of an initially fully separated design.The red and blue lines are stream lines for the hot and cold fluid respectively.

4.3. INTERFACE WALL

The tracking of ψ did not solve completely the problem of hot fluid 'leaking' to the cold flow. In an effort to prevent this phenomenon we introduced an interface wall between the two flows, at the location where ψ becomes zero. As a result the hot fluid will have to pass through the wall in order to obtain positive values of ψ, which will require a great amount of pressure drop. Due to that, the flows are completely separated, satisfying the requirement of a non mixing heat exchanger.
This concept was implemented by redefining the design variable γ as follows:

$$\gamma_{new} = \Pi_{-\psi_0,\psi_0}(\psi)(1-\gamma)+\gamma, \tag{4.4}$$

where,

$\Pi_{-\psi_0,\psi_0}(\psi)$ = a continuous boxcar function [35] as shown in figure 4.10,
ψ_0 = the level of psi where the wall appears.

The new design variable creates an impermeable interface structure at the regions where $-\psi_0 \leq \psi \leq \psi_0$ (see figure 4.11). In this case, equations 3.9 and 4.2 become coupled, and non-linear, as a result of the non-linear boxcar function Π. This non-linearity is not desirable since it introduces computational complexity and convergence problems. Furthermore the uniqueness of the solution is not guaranteed. As a matter of fact, infinitely many solutions may exist, if one considers that at the location of the wall the ψ value becomes zero (see figure 4.2b), and at the regions where $\psi = 0$ a wall is created. This means that any configuration where a wall is separating the two flows is a solution of the system. Due to these difficulties the tracking methods were not further investigated, and another method was proposed.

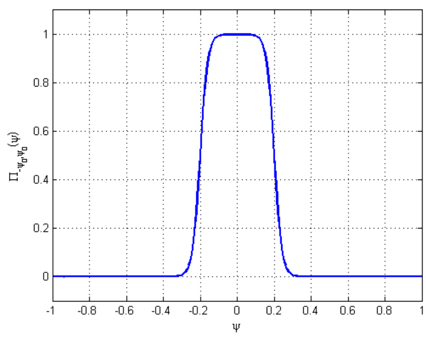

Figure 4.10: Approximate continuous boxcar function $\Pi_{-\psi_0,\psi_0}$ for $\psi_0 = 0.2$. The function takes the value 1 in the region of $-0.2 < \psi < 0.2$, and 0 everywhere else.

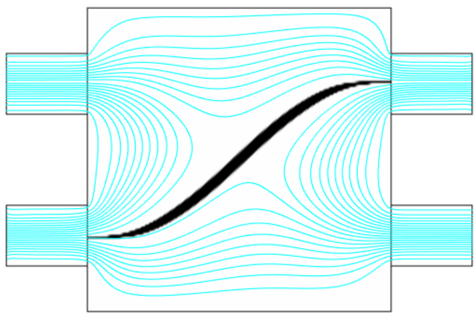

Figure 4.11: Enforced interface wall separating the two flows (black coloured structure).

5

Multi-Material Model

Following the inability of the Tracking Model to produce any useful results, we came up with a different approach to the mixing problem, and introduced a new method called the Multi-Material Method.

5.1. Concept

This method is inspired by the multi-material topology optimization in structural mechanics used in optimizing solid structures that can be build up, using multiple materials [8]. The main characteristic of this multi-material model is the separate flows (i.e. the hot and the cold fluid flow) are assumed to be independent and are also solved separately. Additionally, the design variables control to which flow a region is permeable. As long as a region can be permeable to only one flow, a barrier is formed and non-mixing is inherently guaranteed. Solving the flow separately has the advantage of prescribing the boundary conditions independently, which means that the we can assign a unique inlet and outlet per flow. The remaining inlet and outlet are assigned as solid walls, preventing any short-circuit designs. The two separate solutions of the flows are then added together, forming the complete solution of the velocity field, which is needed for solving the heat problem. The whole procedure of this method can be divided into four separate steps, and is explained in more detail below:

1. The two flow problems are solved separately of each other . The boundary conditions of the problems are assigned independently, but the problems are solved on the entire domain. The two flows can be solved in parallel since they are independent of each other.

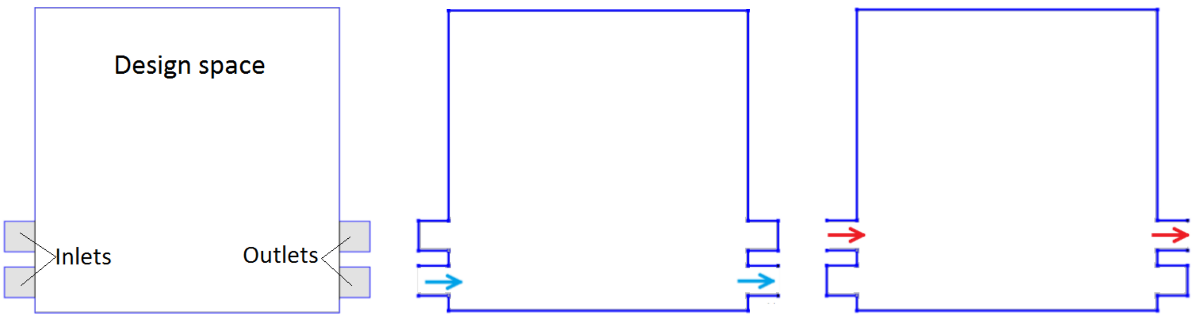

(a) Design space. (b) Cold flow problem. (c) Hot flow problem.

Figure 5.1: Solving the two flow problems separately on the same design space.

2. The velocity fields of the two flows are added to form the combined velocity field solution of the problem.

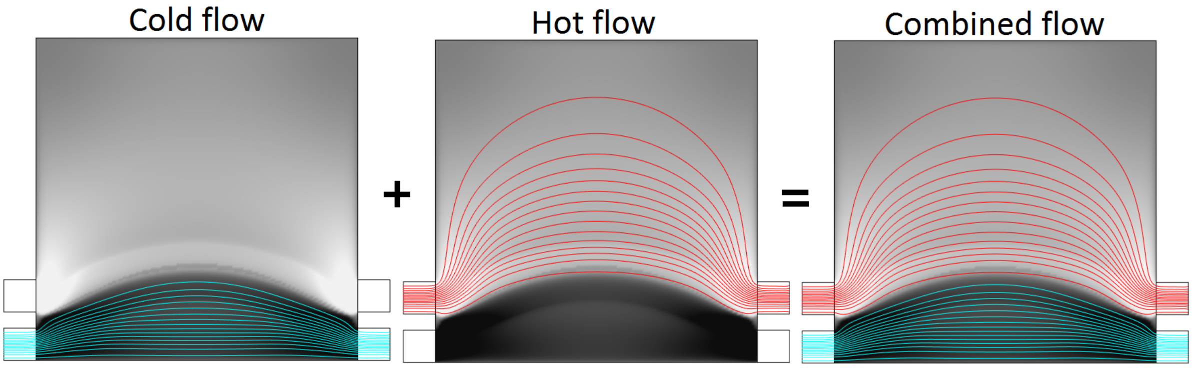

Figure 5.2: Combined velocity field of the two flows. Black areas are permeable regions for the cold fluid (blue stream lines) and white areas are impermeable. The opposite holds for the hot fluid (red stream lines).

3. The heat transfer problem is solved using the calculated combined velocity field

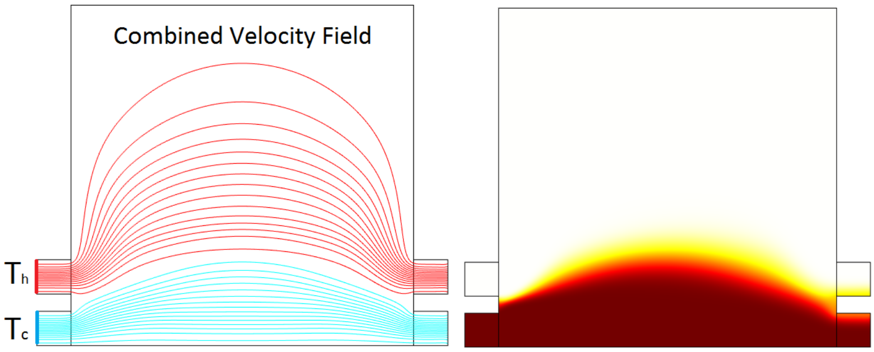

(a) Heat transfer problem of the combined velocity.

(b) Temperature distribution.

Figure 5.3: Temperature field obtained from solving the get transfer problem

4. The optimizer updates the design variables according to the sensitivity analysis that has been performed.

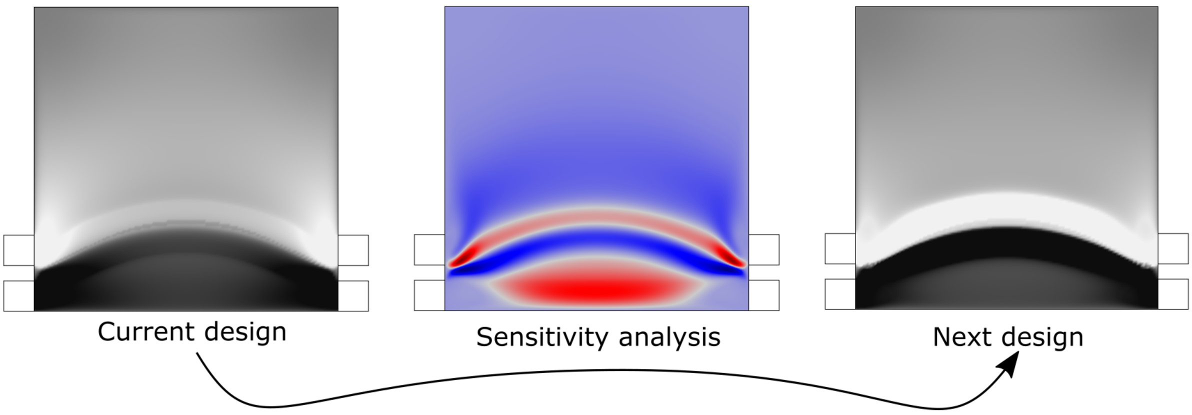

Figure 5.4: Sensitivity analysis of the current design. Blue and red regions indicate where the design should get blacker and whiter respectively.

The permeability of each flow problem is complimentary to the other, which means that when a certain domain is impermeable to one flow it is permeable to the other one and vice versa. As a result, at any given location no more than one fluid can flow, as long as the design variable is at the limits. Intermediate values of the design variable are highly undesirable since they describe semi-permeable regions where flows can intersect (see figure 5.5) .

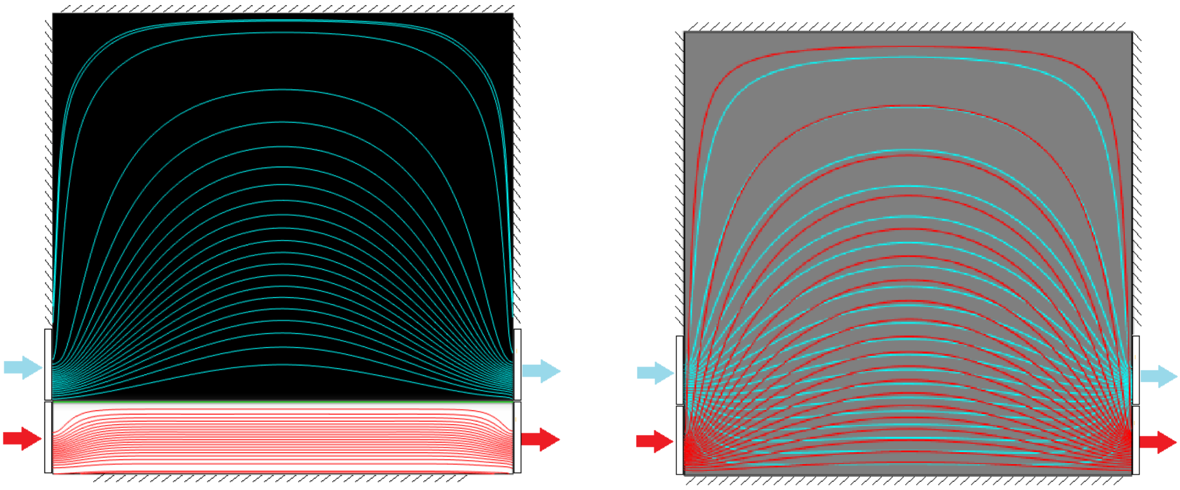

(a) Fully separated flows of a black and white design. The black regions are open areas for the hot fluid and impermeable for the cold one, and vice versa for the black regions.

(b) Intersecting flows of a grey design. Areas of grey colour take intermediate values and represent a semi-permeable state for both fluids. Such design are not desirable.

Figure 5.5: Fully separate flows in a black and white design in comparison to a grey design of mixed flows. The red and cyan lines represent the stream lines of the two different flows.

The below interpolation laws can be used to define the inverse permeability and conductivity as a function of the design variables γ_1 and γ_2:

$$\alpha_1(\gamma_1,\gamma_2) = \alpha_{\text{max}}(1-(1-\gamma_1^{p_1})(1-\gamma_2^{p_2})), \tag{5.1}$$

$$\alpha_2(\gamma_1,\gamma_2) = \alpha_{\text{max}}(1-(1-\gamma_1^{p_1})(1-(1-\gamma_2)^{p_2})), \tag{5.2}$$

$$k(\gamma_1) = k_{\text{fluid}} + k_{\text{solid}}\gamma_1^{q}. \tag{5.3}$$

When $\gamma_1 = 0$ then the problem reduces to an one variable problem. This 2-state model is a simpler version of the 3-state model, that can only represent the fluid-solid states without the ability of a varied conductivity. In figures 5.6 and 5.7 the reader can have a better understanding of the interpolated functions.

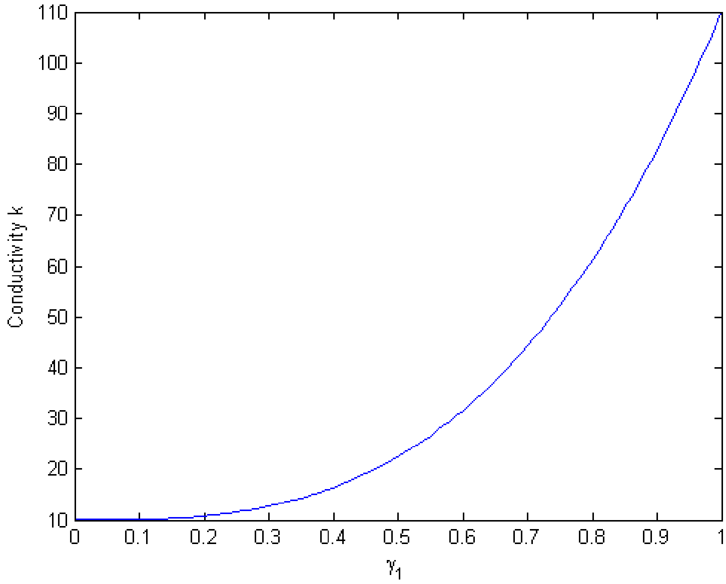

Figure 5.6: Interpolation of conductivity between solid and fluid domain,for $q = 3$. The highest order the polynomial the steepest the function it gets.

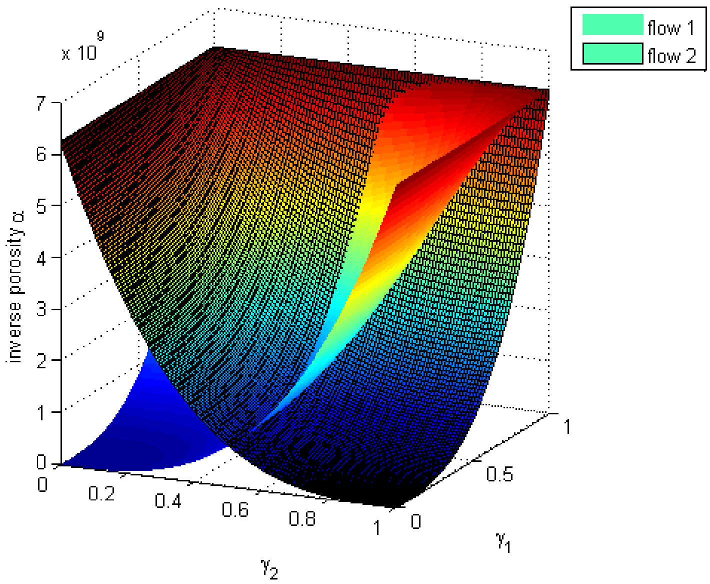

Figure 5.7: Interpolation of the inverse permeability for the two state model for $p_1 = p_2 = 2$.

The two proposed models for heat exchangers are put side to side for comparison in charts 5.8.

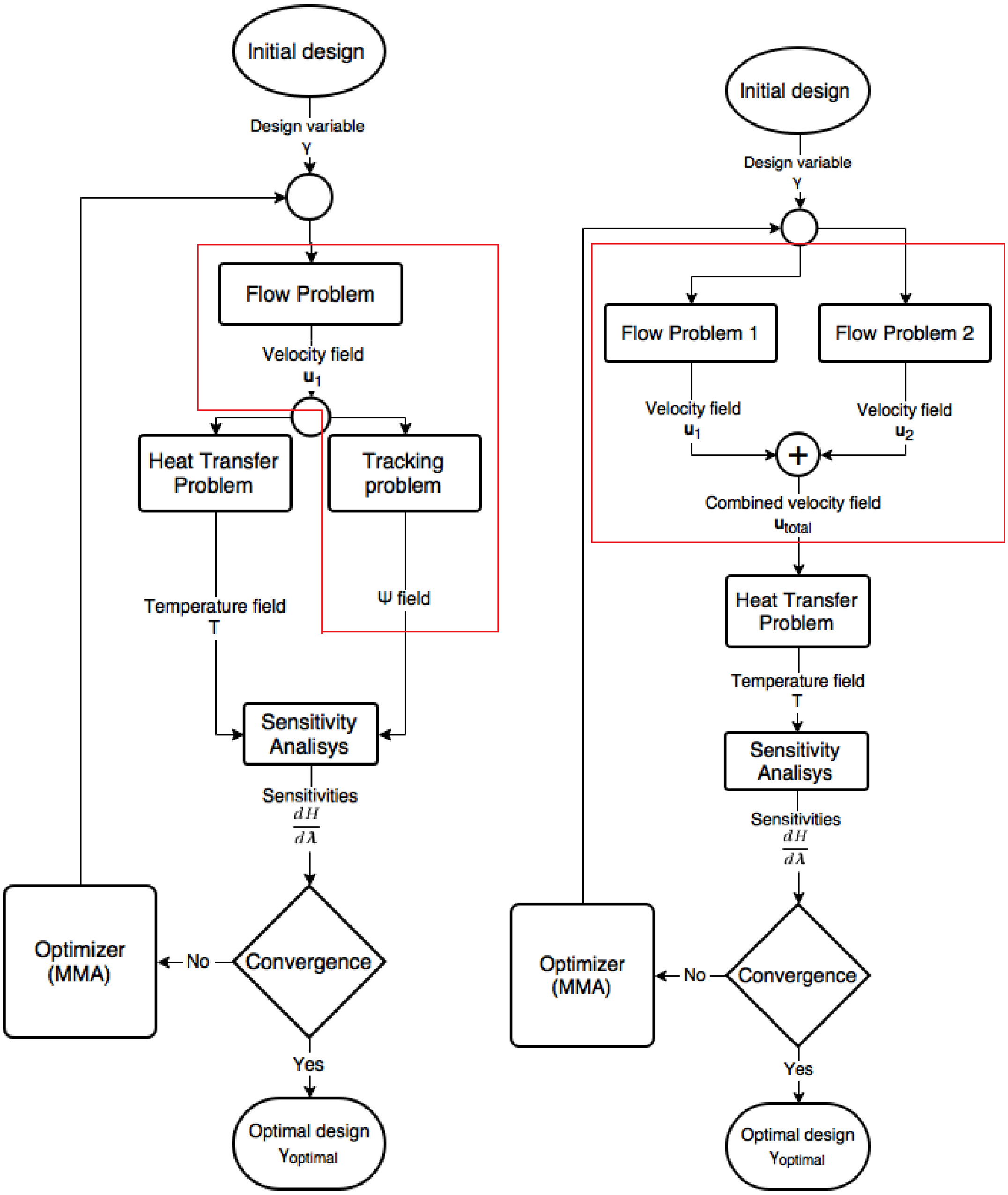

(a) Flow chart of the Tracking Model.

(b) Flow chart of the Multi-Material Model.

Figure 5.8: Flow charts of the two proposed models comparing the steps in each algorithm.

The two method have the same computational complexity, since the number of stages that have to be computed in parallel are the same. The two methods differentiate on the part marked with red colour (see figure 5.8) where the flow problem is solved, and the fluid is tracked. The Multi-Material Model solves a separate flow problem for each set of inlet-outlet, that are coupled by the design variable γ. The tracking of the fluids then becomes unnecessary since the flows exit from a unique outlet by design. The optimizer is no longer able to exploit the mechanism of tracking in order to leak part of the hot flow in the cold outlet, and is able to focus on the natural mechanisms of increasing the heat transfer, such as increasing the length of the channels, decreasing the width, etc. The rest of the steps are the same for both them.

5.2. 2D RESULTS

In this section we investigate the performance of the Multi-Material Model in 2D heat exchanger problems, similar to the ones solved by the Tracking Model. Both 2 and 3 state models are studied for different cases of Reynolds and Peclet number, solid conductivity, counter and parallel heat exchangers, in an effort to check how robust the model is.

5.2.1. PARALLEL FLOW

We consider the parallel flow heat exchanger seen in figure 5.9. The geometry of the domain is slightly different to the one studied in section 3.3, to allow for more complex designs. The inlets and outlets are located at the bottom part of the domain and their width is halved. As in the previous examples the following assumptions were taken:

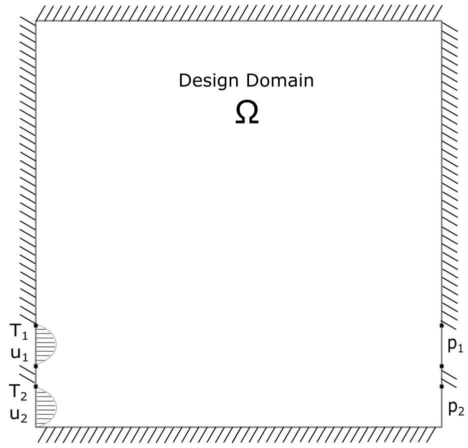

Figure 5.9: Typical boundary value problem of a parallel heat exchanger.

The design domain is a square domain. The two fluids enter from the left side of the domain and exit from the right side. The boundary conditions were taken as follows:

1. Prescribed parabolic velocity profile at the inlets.
2. Prescribed constant temperature at the inlets.
3. Prescribed pressure at the outlets without backflow.
4. No slip condition and zero thermal flux on the rest of the boundaries.

2 STATE MODEL

We consider the case where $\gamma_1 = 0$ which means that we are able to represent only two solid-fluid states. The interpolation functions 5.3 of the permeability and conductivity become:

$$\alpha_1(\gamma_2) = \alpha_{\max}\gamma_2^{p_2}, \tag{5.4}$$
$$\alpha_2(\gamma_2) = \alpha_{\max}(1-\gamma_2)^{p_2}, \tag{5.5}$$
$$k = k_{\text{fluid}}, \tag{5.6}$$

where, the interpolation's polynomial order $p_2 = 5$. Lower values for p_2 produce suboptimal results as it will be explained later in section 5.2.1 (in paragraph: Avoiding infeasible designs). On the other hand increasing the order makes the intermediate values more permeable for both flows, that might result in intersecting flows. The velocity at the inlets, and the conductivity of the fluid were chosen such as the Reynolds number becomes $Re = 0.02$ and the Peclet number becomes $P_L = 20$. The characteristic length was chosen to be the length of the design domain, and the velocity was chosen the average velocity at the inlets, since these quantities are not affected by the change of the topology. We use the Method of Moving Asymptotes (MMA) optimizer (see Svanberg (1987) for details [36]). We used one calculation of the objective function per iteration and we set the internal tolerance factor to 0.1. The optimizer was terminated at a 1000 iterations.

Results: Figure 5.10 shows the optimized results of the heat exchanger. The initial design fully separates the flows as shown in figure 5.10a. The initial design was chosen so that the constraints are not violated. The final optimised design, shown in figure 5.10b, illustrates serpent like, black and white structures, that seem to maximize the surface area of the interface of the two flows, without violating the pressure constraints. As a result of the black and white design, the two flows are fully separated (see figures 5.10e and 5.10f), producing a realistic combined velocity field (figure 5.10g). Most of the conductive heat transfer takes place on the interface of the two fluids, since this is the area with the highest temperature difference (see figure 5.10c). Figure 5.10i shows the temperature profile of the solution and how the temperature layer develops throughout the channel's length.

During the optimization process, the design slowly changed by extending the "solid" structures. Figure 5.10j shows the location of the changes as visualised by the sensitivity analysis. The optimization has not fully converged to an optimum after a 1000 iterations, as seen in figure 5.10k. This plot shows 3 characteristic stages which are related to the optimization procedure. The first stage shows a rapid decrease of the objective function which takes place in the first few iterations. At this point the optimizer rapidly reduces the width of the hot flow channel, bringing the two flows together until the pressure constraint is met. In the second stage, there is a slow change in the objective function. At that point the impermeable structure that is located at the bottom boundary, as it can been in figure 5.10b, is created, and slowly increases in height, making the channels longer. The reason of this slow change is that all the changes happen at the tip of the impermeable structures, as the concentration of the sensitivities indicate. In the third part, a rapid further decrease of the objective happens. At this point the second solid structure on the left boundary begins to develop. Parallel to that, the first solid structure starts to loose volume and transforms to a thin structure.

In general, the optimizer tries to maximize the interface area of the two fluids, by folding them that result to an increased channel length. The length of the interface of the two fluids is bounded, by the design space size and by the maximum pressure drop, which is dictated by the pressure constraint at the inlets. The model seems to behave as expected as established in appendix E

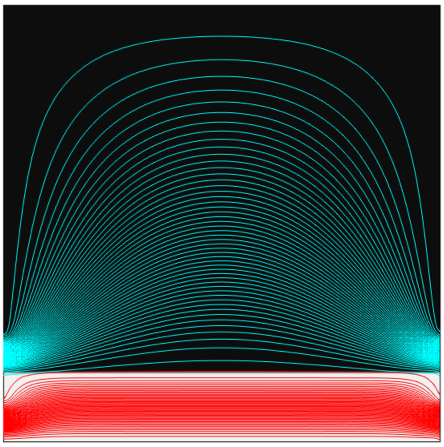

(a) Initial design. The flows start fully separated and the pressure constraint is not violated

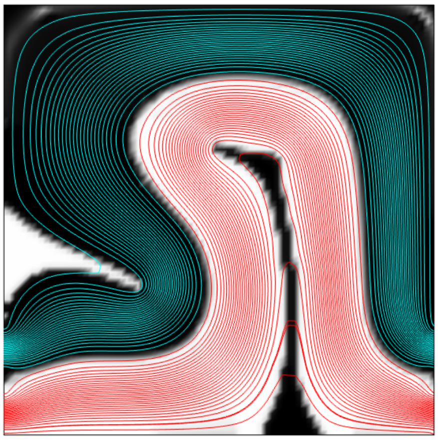

(b) Optimized final design. The design illustrates serpent like channel structures.

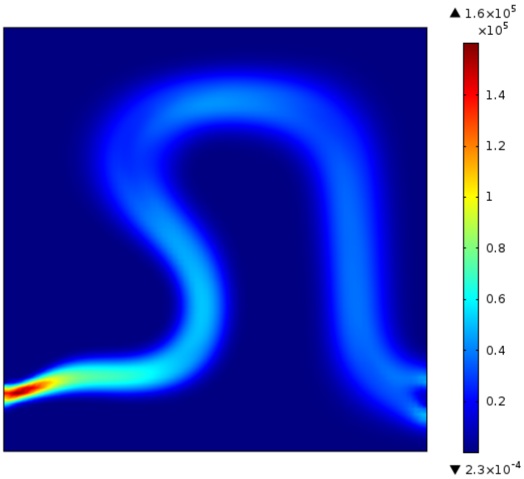

(c) Conductive heat transfer. Most of the conductive heat transfer happens through the interface of the two fluids due to the high temperature gradient.

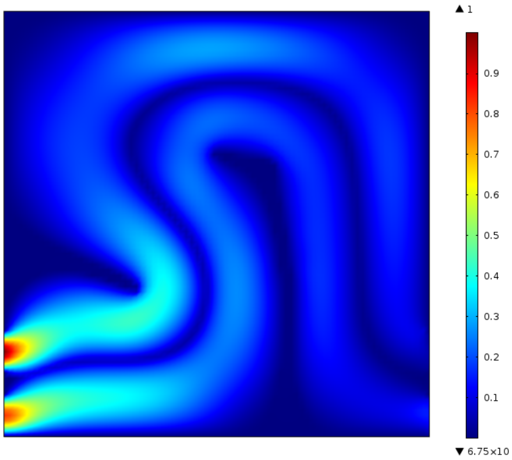

(d) Normalised total energy flux. As the temperature of two flows approach the equilibrium, the energy flux reduces.

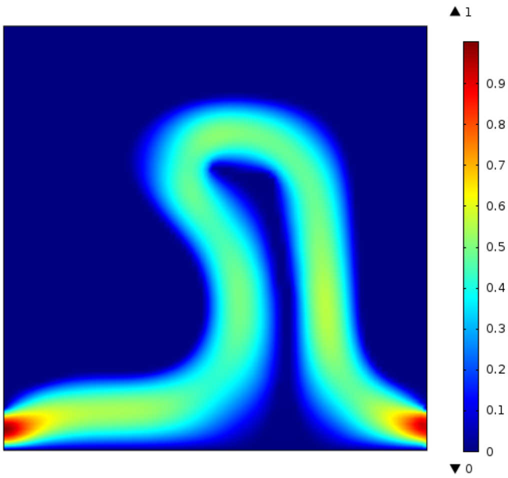

(e) Normalized velocity field of the cold flow. The velocity magnitude approaches zero at the black coloured regions.

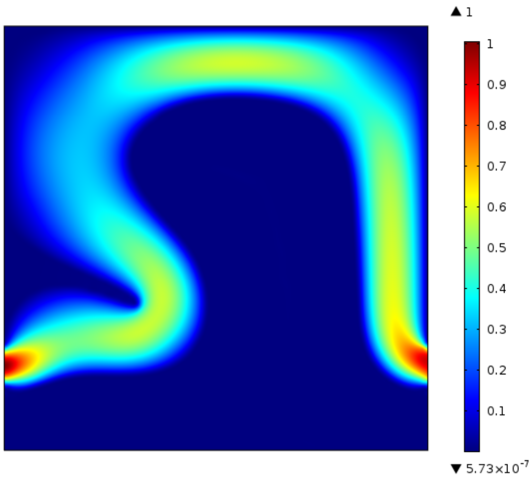

(f) Normalized velocity field of the hot flow. The velocity magnitude approaches zero at the white coloured regions.

Figure 5.10: 2D case of a heat exchanger optimized for maximum heat transfer using multi-material model. The blue and red lines are steam lines of the hot and cold flow respectively. The black and white regions are impermeable to the cold and hot flow respectively.

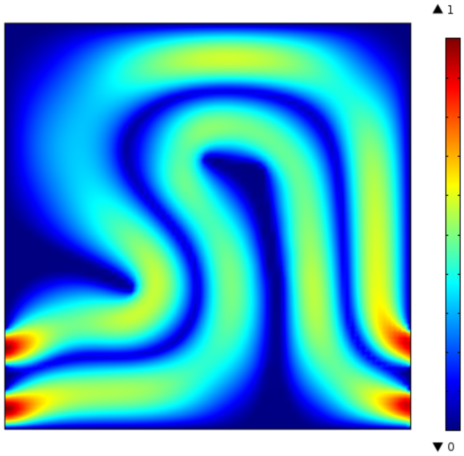

(g) Combined normalized velocity field calculated by adding the two velocity field solutions.

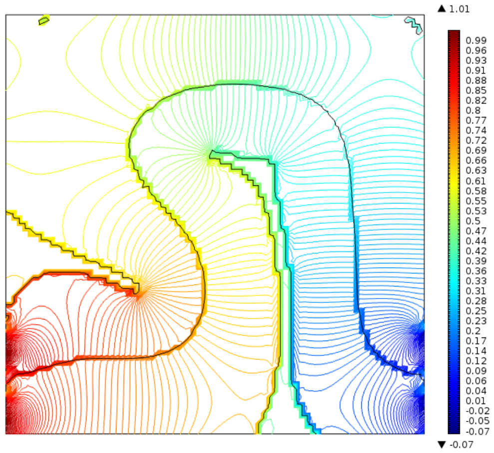

(h) Combined normalised pressure field of the two channels. Pressure spikes appear at the wall structures, due to the large difference of the permeability between the white and the black regions.

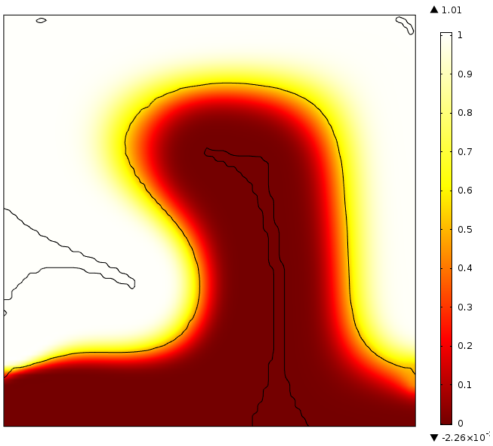

(i) Normalized temperature field. Characteristic thermal layer development of laminar flows.

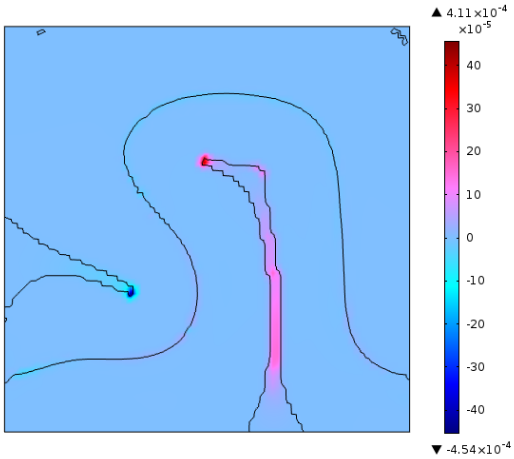

(j) Sensitivity of the objective function. Areas coloured in pink and blue are areas where the optimizer will make more black and more white, respectively, in the next iteration. The design changes by extending the tips of the structures, resulting in increased channel lengths.

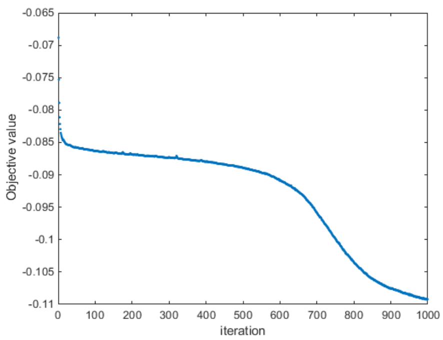

(k) Convergence of optimization. The optimization process reached the iteration limit.

Figure 5.10: Optimal solution of 2-state parallel flow 2D heat exchanger. The black coloured areas are domains where the hot fluid is able to flow 'freely' while the cold fluid is obstructed. The opposite happens for the white coloured areas. Hot and cold flow stream lines are drawn with cyan and red lines accordingly. The final design has not fully converged.

EFFECT OF THE PRESSURE DROP

In this section we investigate the effect of the allowed pressure drop, in our effort to create designs with more complex structures. The Stokes equation for the flow 2.4 shows that the pressure drop is dependent on the gradient of the velocity and the viscosity. This means that increasing the viscosity is equivalent to decreasing the maximum pressure drop allowed. This is valid for Stokes flow, since the inertia forces are neglected.
We solved the same problem for a number of viscosity values to test if decreasing the viscosity would lead to longer and more complex structures. The results can be seen in figure 5.11.

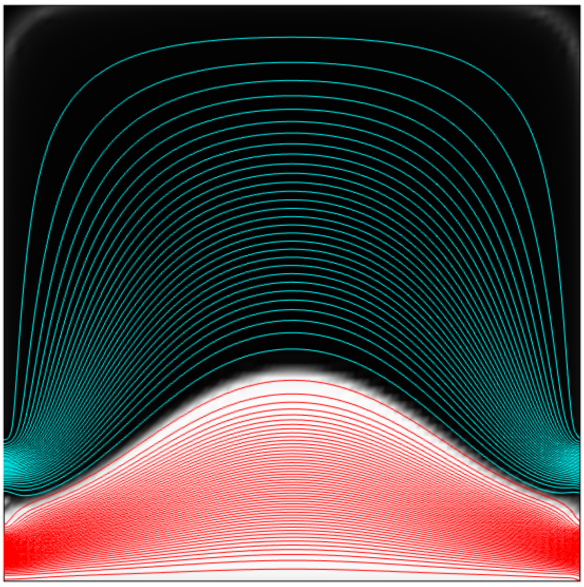

(a) $Re = 0.004$. 5.75 % thermal energy transferred.

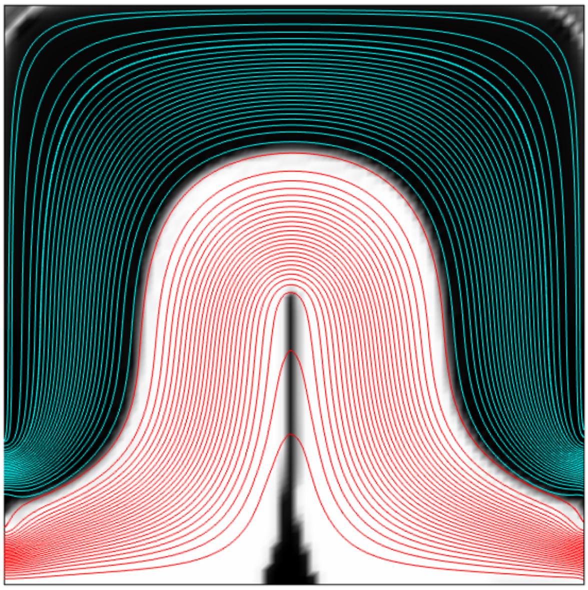

(b) $Re = 0.01$. 6.7 % thermal energy transferred.

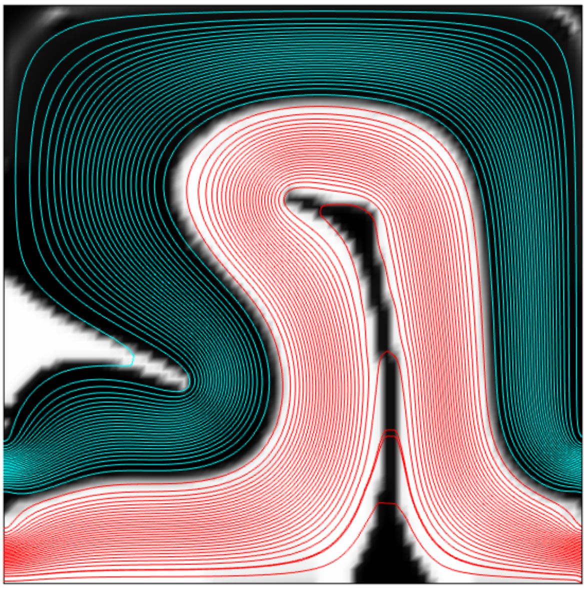

(c) $Re = 0.02$. 10.9 % thermal energy transferred.

(d) $Re = 0.04$. 14.25 % thermal energy transferred.

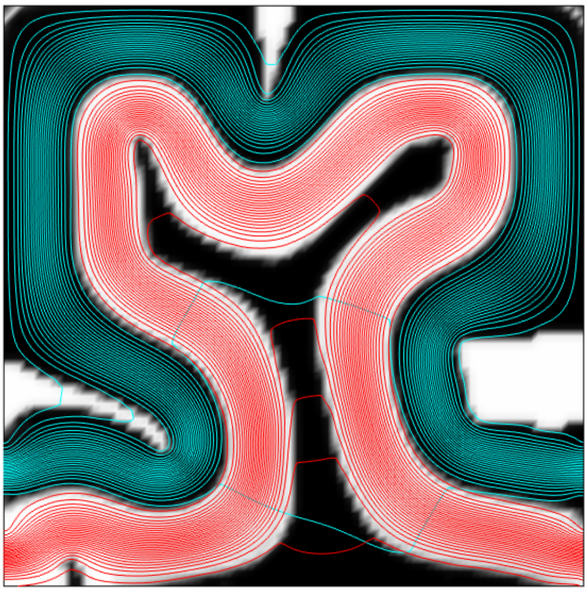

(e) $Re = 0.06$. 16.172 % thermal energy transferred.

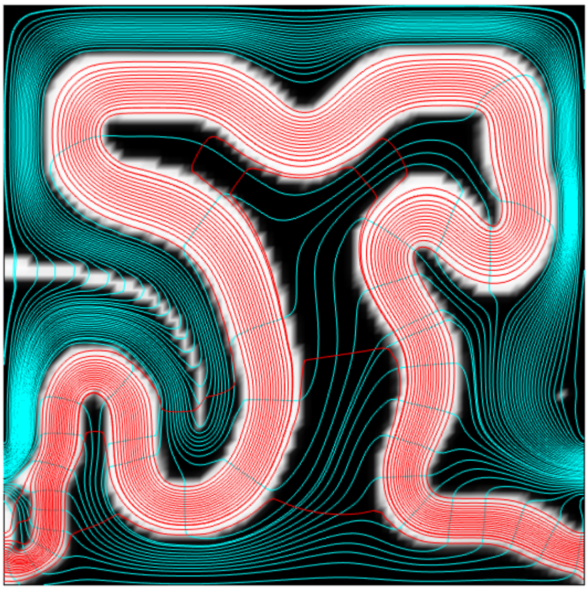

(f) $Re = 0.2$. 23.03 % thermal energy transferred. The hot and cold flows intersect leading to unrealistic designs.

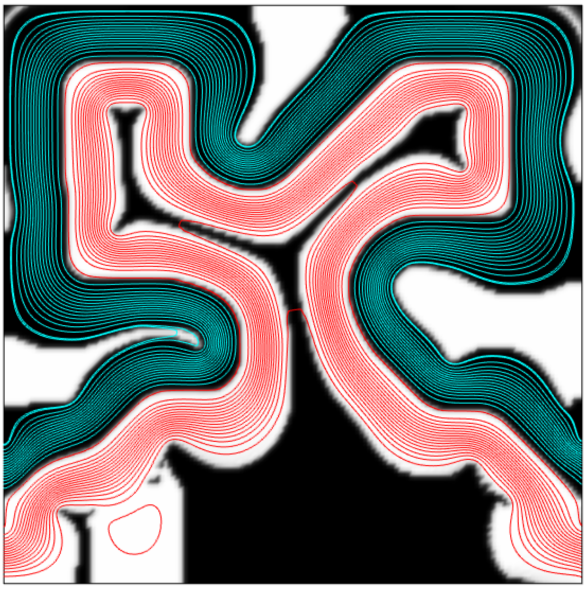

(g) Optimal solution for the reduced order interpolation function. Viscosity 0.1. 20.46 % thermal energy transferred. The design does not seem to converge to a local minimum.

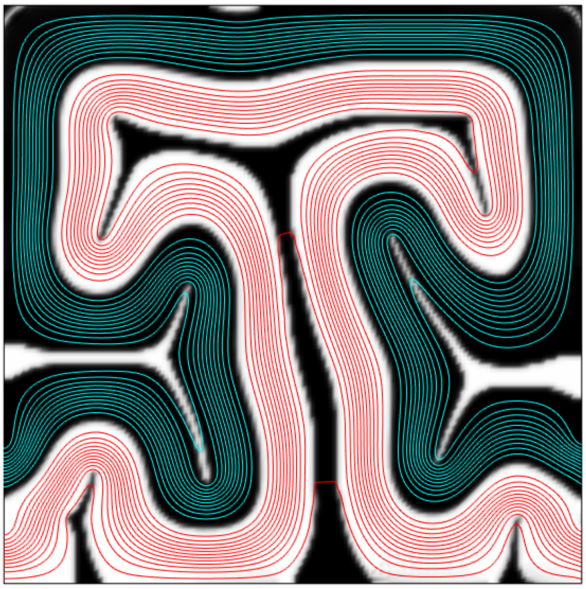

(h) Optimal solution for increased maximum inverse permeability. Viscosity 0.1. 22.14 % thermal energy transferred. The final design makes full use of the design space.

Figure 5.11: Comparison of optimal designs for varied viscosity that translates to varied pressure drop. Red and blue lines are cold and hot fluid stream lines respectively. As the viscosity increases, so does the channel width, in order to meet the pressure constraint.

(a) In figure 5.11a the design is driven by the pressure drop constraint. The cross section area of the channels is increased, such as the pressure constraint at the inlets is met. This is the upper limit for the viscosity, since further increasing it would violate the pressure constraint, no matter the design. The Reynolds number of the flows is $Re = 0.004$.

(b) In figure 5.11b the viscosity is decreased and as a result the channels become narrower and longer, resulting in an increased interface length. The Reynolds number of the flows is $Re = 0.01$.

(c) In figure 5.11c we see the problem studied in section 5.2.1, where the Reynolds number of the flows is $Re = 0.02$. We can see that a further decrease of the viscosity results in an increased interface length. The same patten is seen in figures 5.11d and 5.11e as well, where the Reynolds number is $Re = 0.04$ and $Re = 0.06$ respectively.

(d) Figure 5.11f shows an unrealistic design, where the two flows intersect. The optimizer forces a stream of hot fluid through the cold fluid channel, heating the channel on both sides. This is caused due to a phenomenon known as "leaking walls" caused by the fact the the solid area is not totally impermeable. The narrow channels of the resulted designs, as well as the appearance of slightly grey areas give rise to this phenomenon. The Reynolds number of the flows is $Re = 0.2$.

In general we see that as we decrease the viscosity which translates into an effective smaller pressure drop, the channel become longer and thinner, which in turns increases the heat transfer.

Avoiding infeasible designs: We saw that the optimized design of the problem of figure 5.11f is unrealistic, due to the flows intersecting each other. The intersection flows can be avoided by reducing the order of the interpolation polynomial of the permeabilities, or by increasing the maximum inverse permeabilities. The two proposed solutions are shown in figures 5.11g and 5.11h.

(a) Decreasing the interpolation function of the permeabilities to a 4th order polynomial, results in slower convergence rate and in a suboptimal design, as seen in figure 5.11g. The design does not make full use of the design domain and as a result the length is not maximised. The behaviour of lower order interpolation functions is not well understood yet.

(b) Increasing the maximum inverse permeability the problem, as shown in figure 5.11h), without producing a suboptimal solution. Nevertheless this can result in increased numerical errors, due to ill conditioning.

The effect of the viscosity and as a result the Reynolds number, to the heat transfer can be seen in figure. It is clear that as the Reynolds number increases, so does the heat transfer.

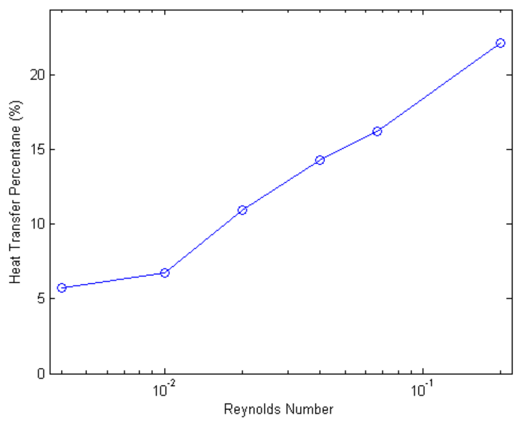

Figure 5.12: Effect of Reynolds number to the heat transfer.

EFFECT OF PECLET NUMBER

The robustness of the Multi-Material Model was also tested in the case of varying the Peclet number. We did this by varying the conductivity of the fluid. Figure 5.13 shows the results of the heat exchanger described by a Peclet number of $P_L = 2$. The final result shows little differences to the problem where the Peclet number is 10 times higher. This is expected in cases where the Peclet number is low enough so the two fluids do not reach an equilibrium, since the optimizer will try to maximize the length of the channels.

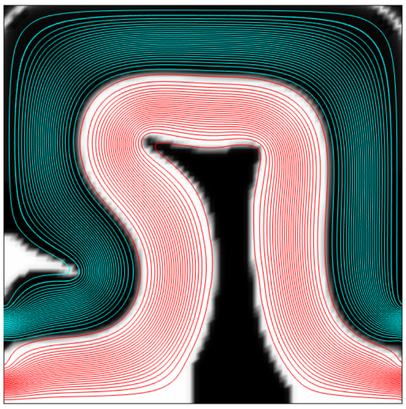

(a) Final design, shows similar structures to the designs pf a lower Peclet number.

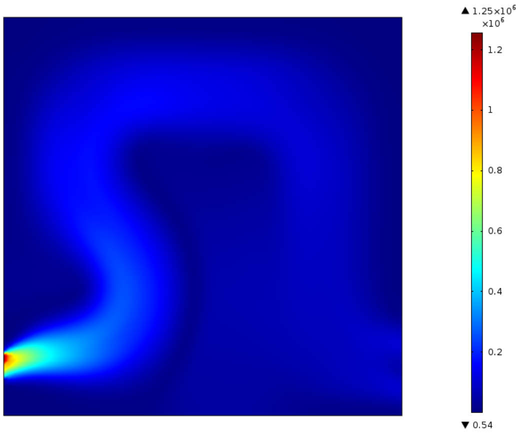

(b) Conductive heat transfer. Most of the heat transfer happens at the entrance of the two fluids

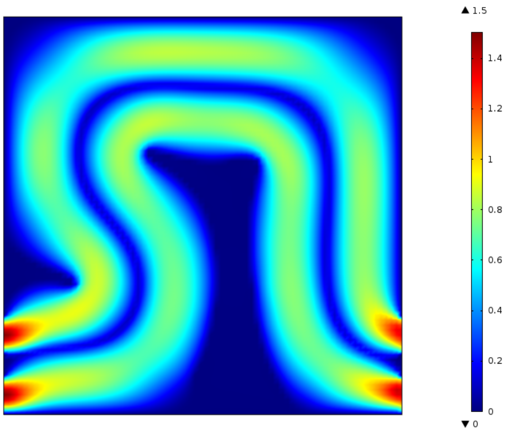

(c) Combined normalized velocity field.

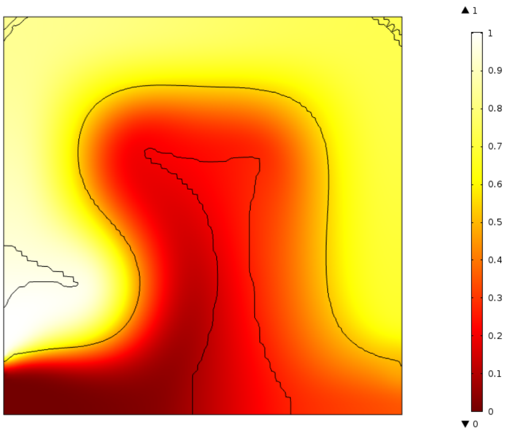

(d) Normalized temperature field.

Figure 5.13: Optimization of a heat exchanger of $Pe = 2$. This design achieves 39% thermal energy transfer.

By increasing the conductivity further the optimizer produces a design with a unexpected topology (see figure 5.14). The design does not make full use of the design space.

What is evident from figure 5.14d is that the two fluids exit with a higher temperature than the average. This implies that the actual energy coming out of the system, in the form of enthalpy, is greater than the energy getting in the system by advective means. Considering the conservation of energy we get:

$$\dot{q}_{in} = \dot{q}_{out} - \dot{q}_{generated}. \tag{5.7}$$

For an insulated heat exchanger, equation 5.7 reduces to an enthalpy balance:[17]

$$((\dot{m}h)_{hot} + (\dot{m}h)_{cold})_{in} = ((\dot{m}h)_{hot} + (\dot{m}h)_{cold})_{out} - \dot{q}_{generated}. \tag{5.8}$$

The mass influx is:

$$\dot{m} = \mathbf{u}A.$$

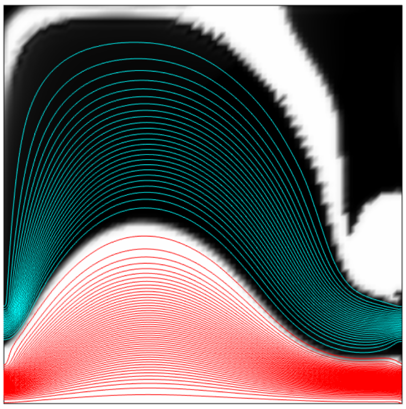

(a) Optimized design. The optimal solution does not make full use of the design space

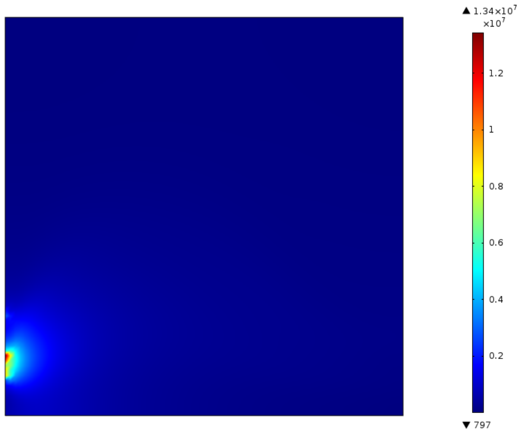

(b) Conductive heat transfer. High concentration of heat transfer at the inlets area

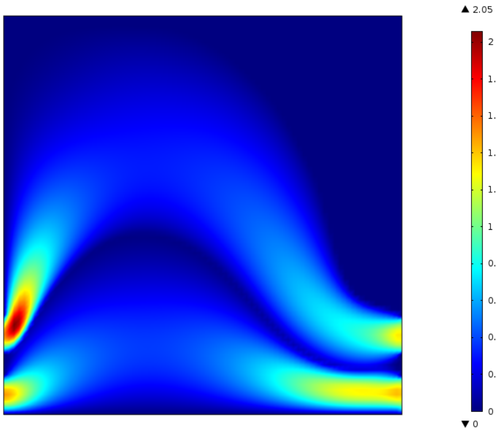

(c) Combined normalized velocity field.

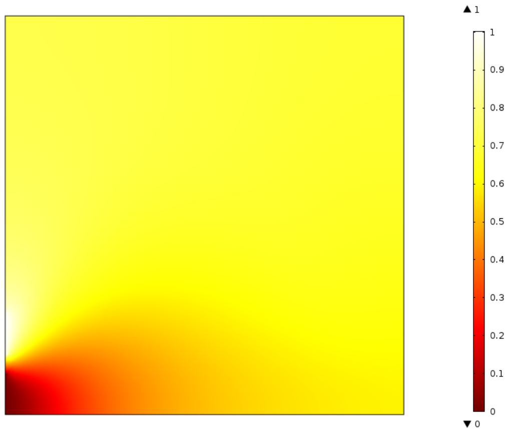

(d) Normalized temperature field. The two flows exit with a higher temperature than the average

Figure 5.14: Optimization of a heat exchanger with $Pe = 0.2$. The conductive heat transfer becomes prevalent to the advective heat transfer

Considering that the inlets and outlets have the same dimensions, both fluids have the same heat capacity c_p, and no heat is generated, equation 5.8 is equivalent to:

$$((\mathbf{u}T)_{hot} + (\mathbf{u}T)_{cold})_{in} = ((\mathbf{u}T)_{hot} + (\mathbf{u}T)_{cold})_{out} \tag{5.9}$$

According to equation 5.9 approximately 15 % more thermal energy exits the system than enters. The "extra" energy exiting from the system is due to the fact that we didn't take into account the energy influx due to conduction from the inlets. According to Fourier's Law 2.7, the heat flux due to conduction is proportional to the conductivity and the temperature difference, and inversely proportional to the thickness of the conductive medium. This means that there is large heat influx generated from the boundary due to the high conductivity, and the low distance between the two inlets. A simple solution to this phenomenon is to add an extension to the inlets of a low conductive medium. Figure 5.16, shows the implementation of the extended inlets to the design shown in figure 5.14. Both of the flows exit with the same average temperature reaching the maximum theoretical efficiency of 50 %. At this high Peclet number the maximum efficiency is reached by such a naive design. The optimizer no longer tries to increase the length since the global optimum is reached. Figure 5.15 shows how Peclet number affects the thermal energy transferred from the hot flow to the cold one.

3 STATE MODEL

In this section we will test the 3 state model **(fluid-solid, solid-fluid, solid-solid)**, as formulated in equation 5.3. The additional design variable allows for an extra solid-solid state, and for a varied conductivity. We

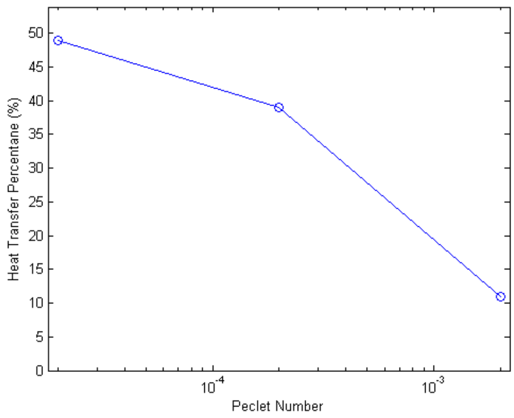

Figure 5.15: Effect of the Peclet number on the heat transfer.

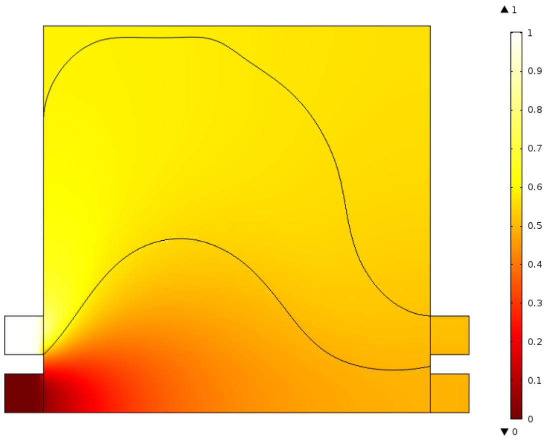

Figure 5.16: Temperature profile of the extended inlets problem. Both of the fluids exit with the average temperature of the inlets, the heat equilibrium is restored.

tested the 3 state model on the problem seen in figure 5.10 in order to see how does the extra state affect the final solution. The conductivity of the solid state was chosen to be 10 times higher than the fluid's. The rest of the parameters of the problem were kept the same.

Results The resulted topology of the design is very similar to the 2 state model. The only difference can be found at the structures that direct the flows, as in the 3 state model are made of higher conductive material. This seems logical as it allows for a better heat transfer between the different segments of the same channel. No fin like structures appeared on the interface of the two flow. We see that the introduction of the higher conductive solid state had little effect on the final design. A similar solution was obtained when starting from a different initial design (see figure figure5.18). This means that many local minimums exist, since the optimal width/length channel ratio can be achieved in many designs.

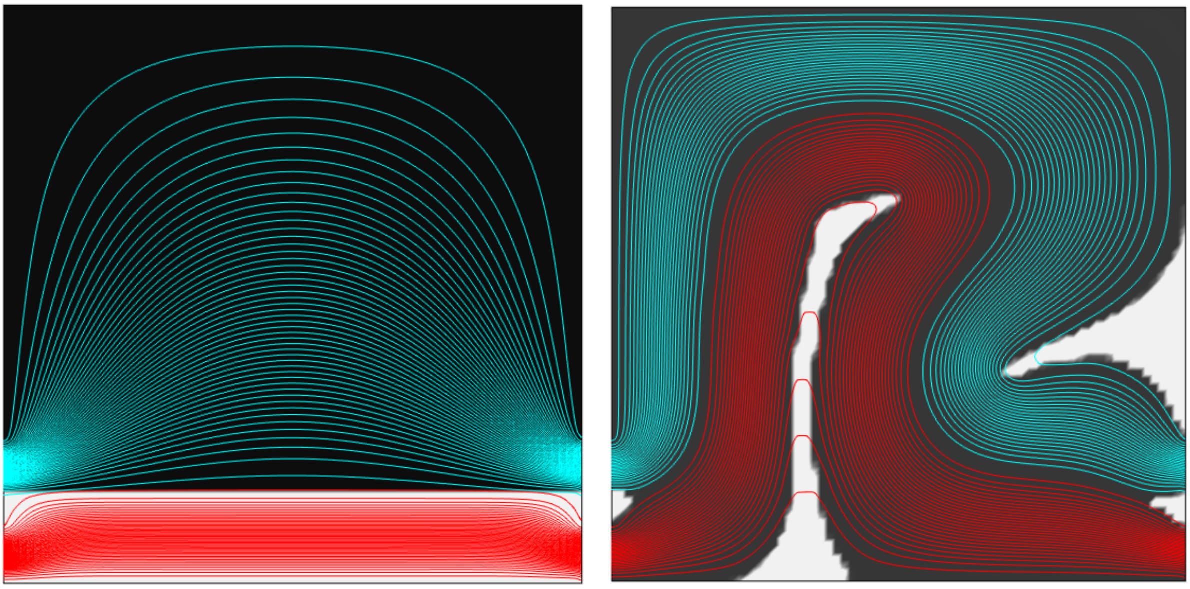

(a) Initial values of the design variable γ_2. The two flows start completely separated

(b) γ_1 field and the stream lines of the optimized solution. The white regions are regions where solid of high conductive solid material, while the black one is not.

Figure 5.17: Optimized solution of 3-state parallel flow 2D heat exchanger. 10.92 % thermal energy transfered to the cold flow.

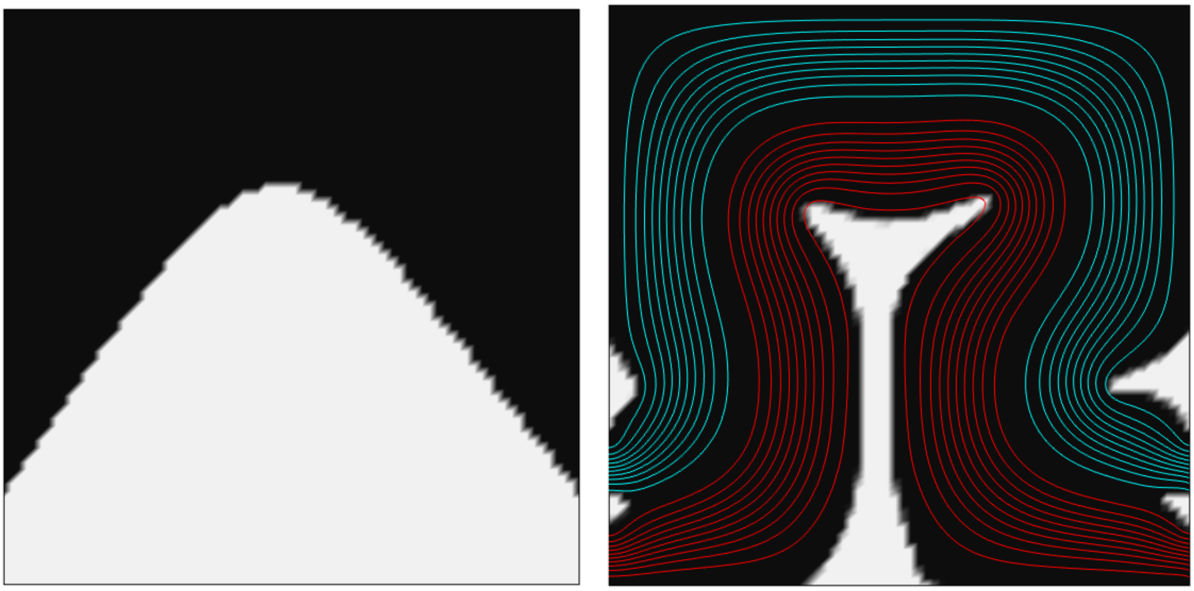

(a) Initial values of the design variable γ_2. The two flows start completely separated.

(b) γ_1 field and the stream lines of the optimized solution. The white regions are regions where solid of high conductive solid material, while the black one is not.

Figure 5.18: Optimal design for a different initial design.

Effect of Higher Conductivity of the Solid State In this section we study the effect the conductivity of the solid state on final design. We increased the conductivity of the solid to a 1000 times higher than the conductivity of the fluid. In order to avoid the conductive heat flux due to the temperature boundary conditions, as explained in section 5.2.1, we introduced low conductivity extensions at the inlets.

Figure 5.19a shows the final result of the optimization process of such a heat exchanger. The most obvious change in the design is the creation of a solid structure at the interface of the two flows. This increases the length of the top channel, while the bottom one does not have any increase in length. Nevertheless this allows for a smaller width for the bottom channel that increase the heat transfer as explained in section E. Nevertheless the design seems to be suboptimal compared to the serpent like channel structures (see appendix C).

Moreover grey areas appear as a consequence of the two properties being dependent on the design variable. The grey areas are of relatively high permeability and considerable high conductivity resulting in highly conductive semi-permeable flow regimes. For such big differences in the conductivity of the fluid and solid it would be more appropriate to use a higher order polynomial for the conductivity interpolation to avoid these grey states. The thermal energy transfer achieved is higher than the previous problem (see figure 5.17), due to the presence of intermediate values of the design variable. The reason for this suboptimal design can either be it being a local minimum or the optimizer exploiting the intermediate values of the conductivity. We further see in figure 5.19b that the solid region has an almost constant temperature profile as a consequence of the high conductivity.

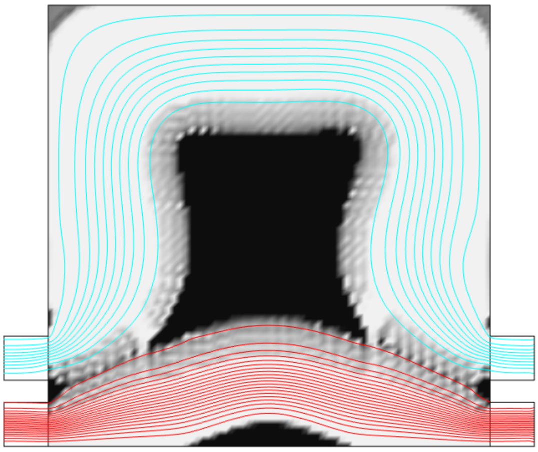

(a) γ_1 field and the stream lines of the optimized solution. The white regions are regions where solid of high conductive solid material, while the black one is not. The conductivity of the solid is 1000 times higher than the fluid. A big fin like solid structure appears at the interface of the two flows.

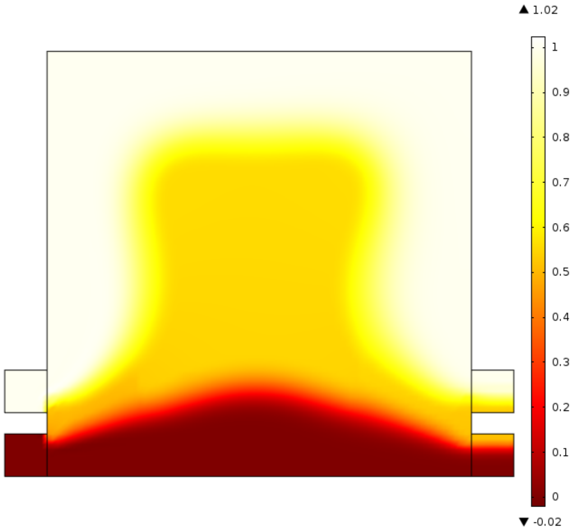

(b) Temperature field of the optimized solution. 14.2% thermal energy transferred to the cold flow.

5.2.2. COUNTER-FLOW

A more widely used heat exchanger is the counter-flow heat exchanger. They can achieve theoretically heat transfer efficiency up to 100%. In these types of heat exchangers the two fluids flow in the opposite directions. This allows for a higher temperature difference between the two flows throughout the system and better efficiency as a result. The optimal configuration of counter-flow heat exchanger is not always intuitive and straight forward as it is in the parallel flow heat exchanger, even in the simpler 2D cases. Such a case is the optimal conductivity of the wall as explained in appendix D.

3-STATE MODEL

The counter flow heat exchanger problem that we study, shares the same geometry as the parallel ones but with interchanged the hot inlet and outlet (see figure 5.20a). The Reynolds and Peclet number are $R_e = 0.02$ $P_L = 20$, respectively and the conductivity of the solid material is 10 times higher than the fluid's.

Results The results of the optimization are shown in figure 5.20. The resulted design resembles the one of the parallel heat exchanger (see figures 5.20 and 5.17). The main difference is that the structures that direct the flow are not made of highly conductive material. The reason of this is not yet clear. As expected the counterflow design outperforms the equivalent parallel flow design (see figure 5.17), achieving 26% higher efficiency.

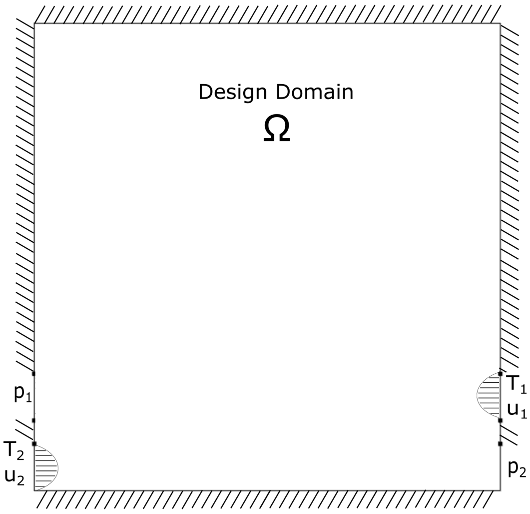

(a) Design domain and boundary conditions of a counter heat exchanger.

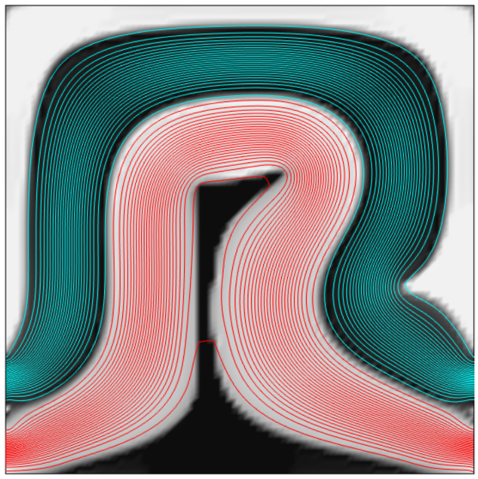

(b) γ_2 field of optimal design. White and black areas behave as walls for cold and hot flow respectively.

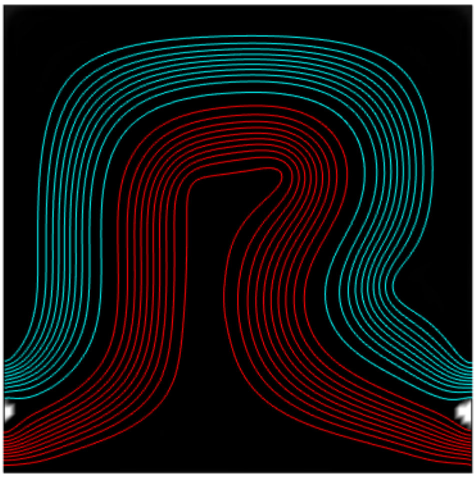

(c) γ_1 field of optimal design. White areas represent the solid state of the domain. There is hardly any solid region, due to the phenomenon explained in appendix D.

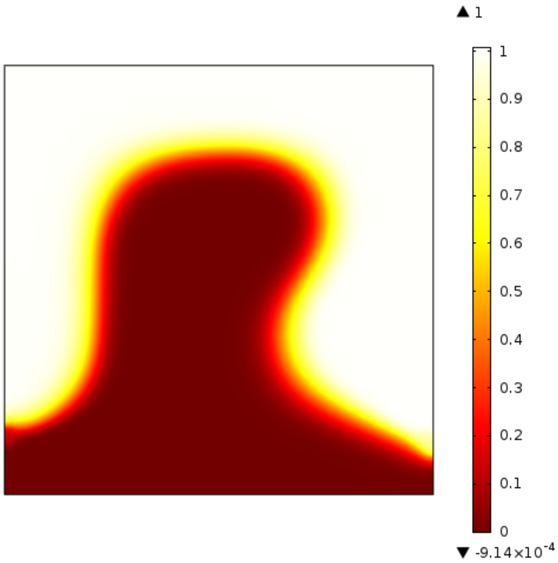

(d) Normalized temperature field.

Figure 5.20: Optimal solution of a counter flow 2D heat exchanger. 13.75 % thermal energy transferred.

5.3. 3D RESULTS

In the previous chapter we tested the multi-material model in 2D problems. The results gave us more insight about the mechanisms of increasing the heat transfer. We saw that constricting the design to a 2D space prevents the fluids from bridging each other and does not favour the creation of fins. The next logical step is to move to 3 dimensions, in order to allow for more complex channel structures. 3D problems are considerably computationally more expensive than 2D problems (the complexity is n^3), both time and memory wise. Because of these limitations coarser meshes were used than in 2D cases (see figure 5.24b), that decrease the accuracy of the solution, and the ability of creating fine structures. Furthermore less iterations were used in 3D; 100 iterations in comparison to the 1000 iterations used in the 2D problems.

5.3.1. PROBLEM 1

The problem that we studied is that of a coaxial cylindrical parallel heat exchanger. The design space is a cylinder with a diameter to length ratio of $\frac{5}{6}$. The flow's Reynolds number was set to be $Re = 0.01$ and the Peclet number $P_L = 600$. We chose the order of the polynomials of the equation 5.3 to be: $p_1 = 1, p_2 = 3, q = 5$, so that the intermediate values of the design variables become unattractive to the optimizer. We used a higher order polynomial for interpolating the conductivity, so that we could avoid the grey regions encountered in section 5.2.1. The conductivity of the solid was chosen to be 1000 times higher than the conductivity of the fluid, so that fin structures are more likely to be created as in the 2D case 5.2.1

The first problem was affected by the boundary heat flux that we encountered in the 2D case (see section 5.2.1), which at that time we were unaware of. Although the problem is flawed, the design illustrates some interesting channel structures, as shown in figure 5.23. The two flows form intermixing channels. It is difficult to understand the topology just by looking at the isosurface of the design variable in figure 5.22. Nevertheless the velocity plot in figure 5.23 clearly shows that the interface wall creates entangling channels of the two fluids.

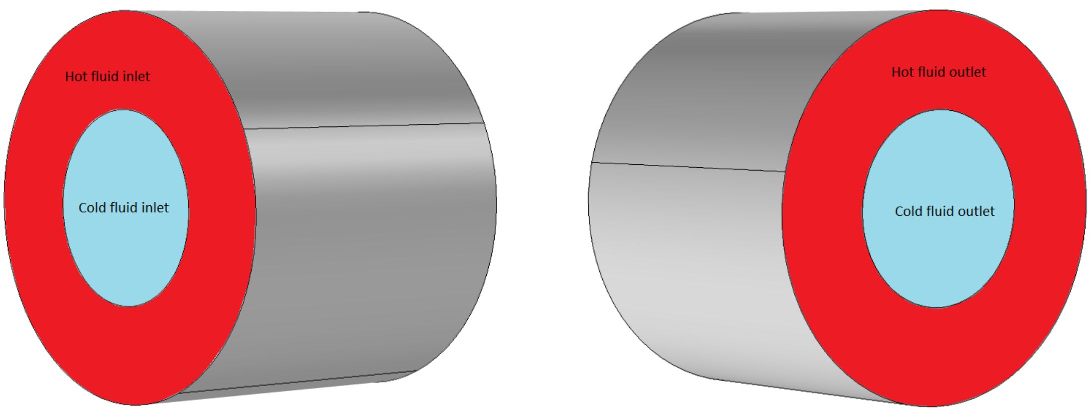

(a) Inlets of the heat exchanger. (b) Outlets of the heat exchanger.

Figure 5.21: 3D domain.

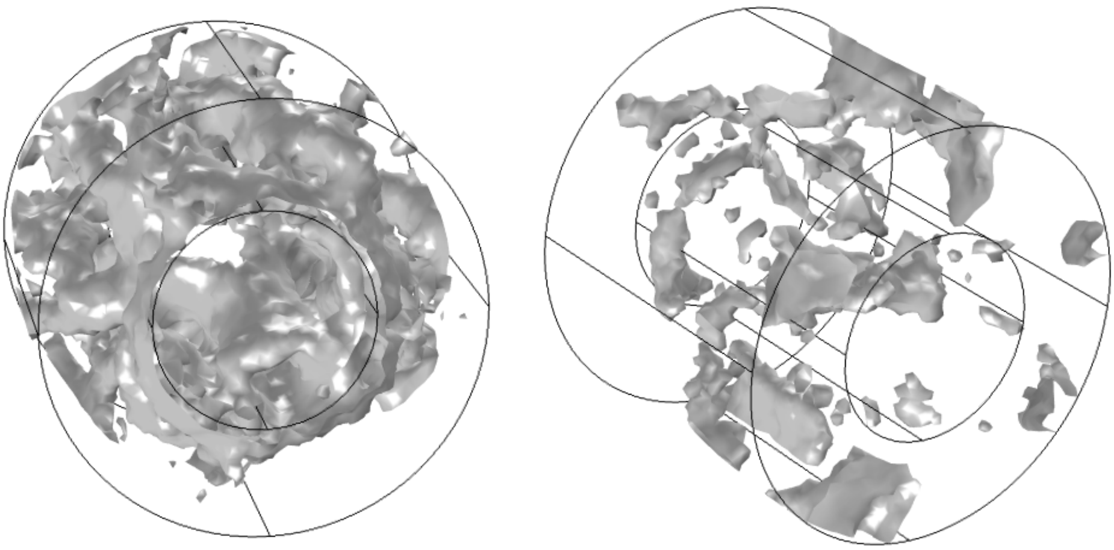

(a) Interface wall represented as an isosurface of the γ_2 design variable field.

(b) Solid structures represented as an isosurface of the γ_1 design variable field.

Figure 5.22: The interface wall and the solid structures that appear in the structure create complex channel structures.

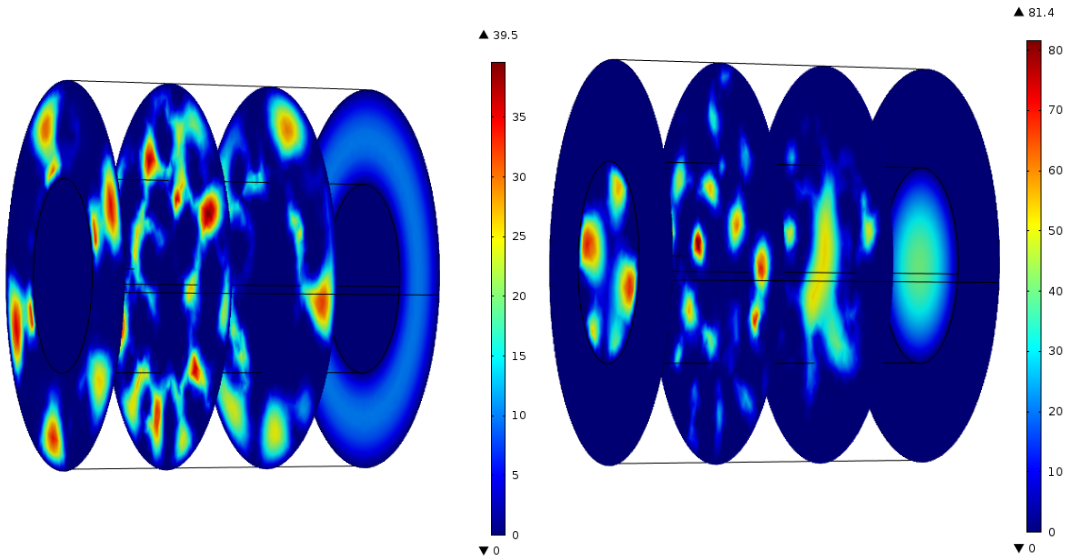

(a) Velocity field of hot fluid.

(b) Velocity field of cold fluid.

Figure 5.23: Velocity fields of the two flows. The two fluids flow through narrow channels that spread across the design space.

5.3.2. PROBLEM 2

We solve the boundary heat flux problem by introducing low conductivity extensions to the inlets, as seen in fig 5.24a. The problem is solved for 100 iterations. The initial values for the design variables was set to 0.5 for both γ_1 and γ_2.

RESULTS

The resulted design did not converge as it can be seen in figure 5.27b, so not many conclusions can be drawn. The optimized result does not illustrate the intertwined channels that we saw in the previous result, probably due to not converging to a local minimum. The two fluids are flowing in two separate regions, as seen in figure 5.25. The outer flow is driven by small radial channels that seem to act counter-intuitively on the notion of maximizing the interface area. On the other hand the topology creates circulation flows (see figure 5.26a) between the channels that possibly increases the convective heat transfer, by circulating the thermal layers. The vorticity plot of figure 5.26b shows how the fluid is transported from on channel to another.

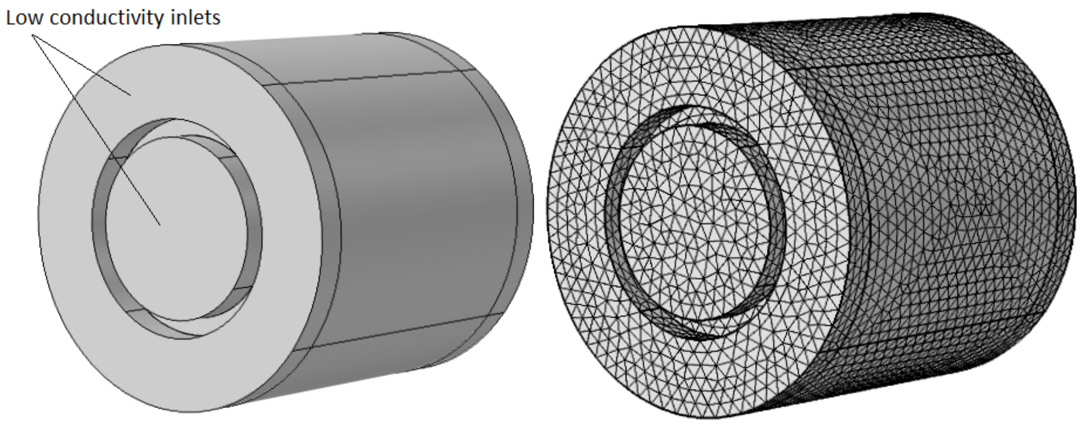

(a) Design domain of 3D heat exchanger. Inlet and outlet extensions of the domain are not part of the design space.

(b) Discretization of the domain using tetrahedron elements. The used mesh is not very fine for flow problems.

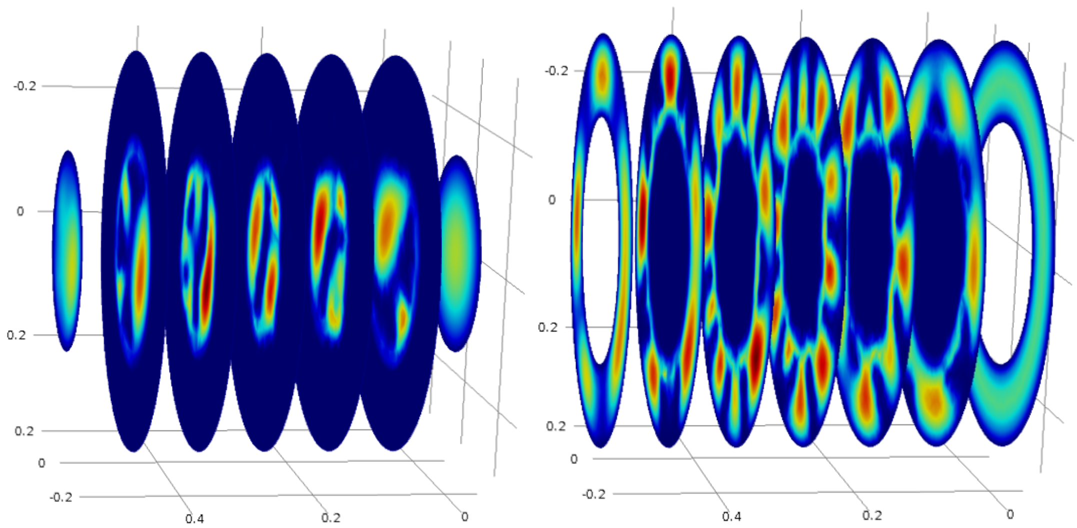

(a) Normalised velocity field of the cold flow. The fluid flows trough two central main channels.

(b) Normalised velocity field of the hot flow. The fluid flows in several small radial channels.

Figure 5.25: Velocity field of the two fluids. The resulted topology keeps the two flow regions separated.

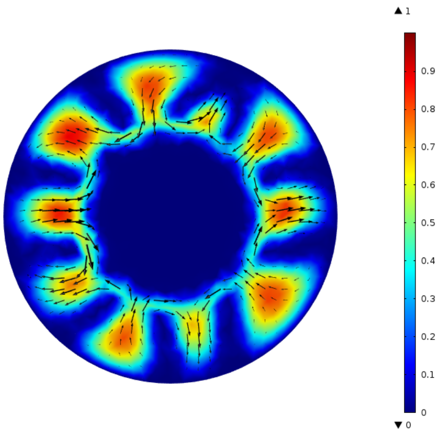

(a) Normalised velocity components of the hot flow normal to the channel's length, show circulation patterns.

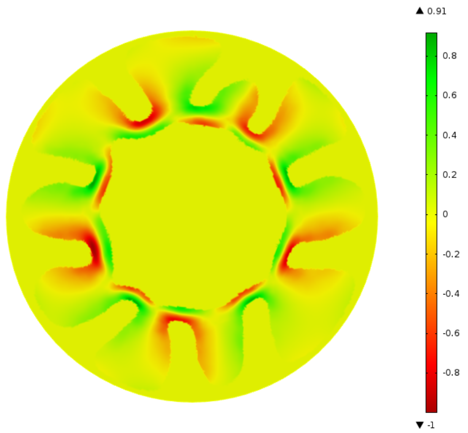

(b) Normalised vorticity of hot flow, normal to the plane.

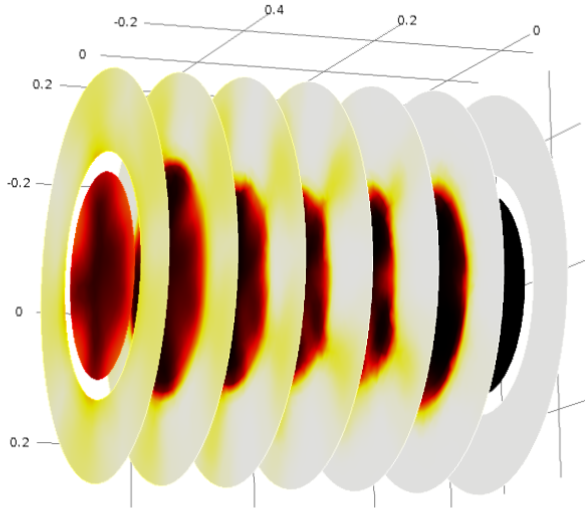

(c) Temperature field. The energy equilibrium holds.

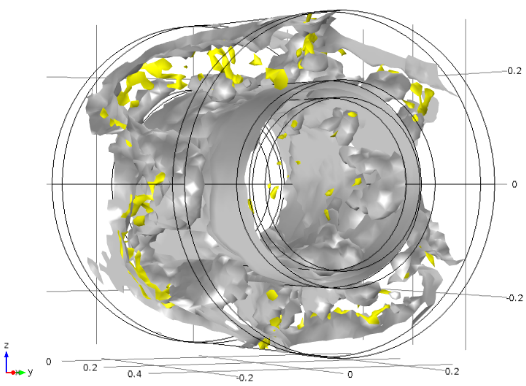

(a) Resulted topology of the interface wall (grey surface) and the solid regions (yellow areas).

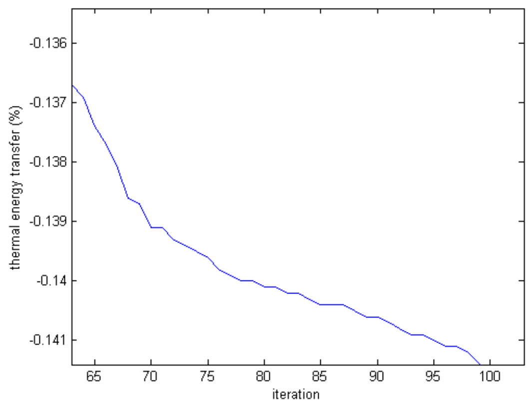

(b) Convergence rate. The problem has not converged to a minimum.

Figure 5.27: Resulted design of the second 3D problem.

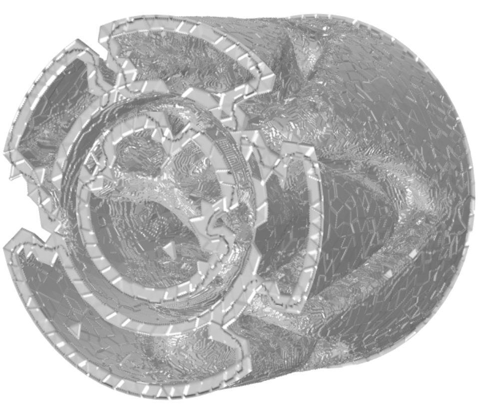

(a) Front view of the post-processed design.

(b) Back view of the post-processed design.

Figure 5.28: Post process design of optimized design 5.27a.

The design in figure 5.27a is not manufacturable since the solid parts of the design are not connected together, and are effectively hovering over the liquid. Further post processing of the design must be done in order to make the design manufacturable. For that purpose we need to connect the hovering solid structures to the boundaries of the domain, as well as add thickness to the interface. The latter was done by considering the areas where the velocity of the fluids is close to zero, to be solid. The resulted design can be seen in figure 5.28. These changes might make the design more realistic, but on the other hand reduce the effective cross section area of the channels, resulting in a completely different topology, thus drifting away from the optimised one.

PERFORMANCE COMPARISON

So far it was easy to evaluate the performance of the optimized 2D heat exchangers, by comparing them to a simple straight channel designs. The same can be done for the 3D optimized designs, but this time a more realistic design can be used for comparison. In order to evaluate the optimized design we compare it to an actual concentric tube heat exchanger. Although these heat exchanger are rarely used in practice, it will be a good indication if the optimized solution is able to perform better than something that is already being used in practice. In order to have a fair comparison between the two designs, the following specifications need to be met:

- The mass flow rate is the same for both designs.
- The temperature that the two fluids enter the system is the same for both designs.
- The design can not extend outside the design domain.
- The pressure drop of the inlets must be the same for both designs.
- The properties of the materials are the same.

Since the design space can not be extended, and taking into account our previous findings on the effect of the length and width on the heat transfer (see section E), we design the tube heat exchanger with the maximum available length and we tune the width of the channels as such we achieve the maximum allowed pressure drop. The tube heat exchanger that complies to the above requirements is shown in figure 5.29. The resulted radius of the tube exchanger is considerably smaller than the available design space.

The heat transfer of the optimized design is moderately better than in the concentric tube heat exchanger-achieving a 14.14 % heat transfer compared to 13.52 % of the tube design. This seems promising if one considers that the solution did not converge. Considering that we use different formulations for the two problems, and the possible discretization error of the coarse grid that was used, the difference is small. A better approach would be to use the same approach for both flow, but extracting the geometry of the 3D problem proved to be troublesome. Our attempt to extract the geometry of the isosurface and edit it in Solidworks was not successful due to the enormous requirements of memory.

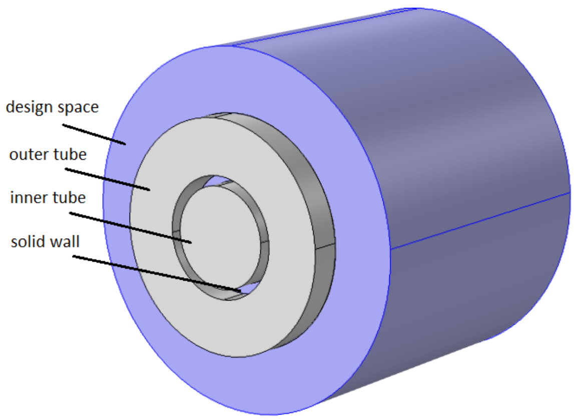

Figure 5.29: Concentric tube heat exchanger that satisfies the pressure drop constraint. In grey appear the concentric tube channels, while blue appears the design space.

6

Conclusion and Further Research

6.1. Conclusion

This thesis investigates and develops a model for topology optimization of non-mixing (fluids separated by walls) multi-flow heat exchangers. The study is focused on heat exchangers described by a relatively low Reynolds number and a high Peclet number. We use the Bringkman formulation of porous media flows to model solid regions (sec.2.6). The optimization objective is the maximization of the thermal energy exchanged between the two fluids. The thermal energy transferred between the two fluids is quantified by the change of the enthalpy of the cold fluid that exits the system (eq.3.6). To the best of my knowledge this study is the first in topologically optimizing a multi-flow heat transfer problem, as all related studies are focused on single flow problems.

Optimizing the topology of single flow heat exchangers is a relevant but simpler version of the same problem. Typical this is solved by using a single set of governing equations to describe the fluid's motion and boundary conditions, assuming a single fluid physics problem (see [27], [11],etc.) Unfortunately in the case of multi flow heat exchangers this method results in short-circuit designs (see section 3.3). This maximizes the enthalpy of the flow that exits from the cold outlet, however it does not maximize the heat transfer between the two flows. Furthermore the design does not comply with the non-mixing requirement, as the two flows came in contact.

We propose two new models to solve these problems, the Fluid Tracking Method (sec. 4) and the Multi-Material Model (sec.5). The latter one shows the best results.

Fluid Tracking Method We introduced a tracking mechanism for the two flows, that allows us to penalise any short-circuit designs. The term *tracking* refers to the process of identifying from which inlet a particular flow region originated.This method eradicated the short-circuit problem, but it did not produce a great heat exchanger. The optimizer exploits the diffusion term for the traced quantity (see section 4) that is required to produce numerically stable solutions. As a result a small portion of the hot flow 'leaked', and exited from the cold outlet. We tried to tackle this problem by introducing a wall region at the interface of the two flows. The implementation of this idea proved to be problematic. For instance, the optimization process became much more erratic and easily got stuck close to the initial design. The above difficulties would require fixes which would undermine the simplicity and generality of the method. Therefore we focused on a solution that would guarantee non-leaking flows.

Multi Material Model In order to get rid of the 'leaking' issue, we move away from the single set of governing equations approach, and use a different set of governing equations for each flow, so that each inlet and outlet is assigned to a specific flow. The Multi Material Model is based on the concept of solving the two flows independently of each other. Each flow is solved for the entire domain. We use a different set of governing equations for each flow making it impossible for a flow to exit through the inlet or outlet of the other flow. This makes sure that flows can never mix and that short circuits can never be beneficial in terms of the objective function. This method is implemented similarly to that of multi-material topology optimization in structural mechanics. The design variables now control whether a region is permeable for either one flow or the other, or to none of them (see Bendsoe et al. [8]). This model solves the short circuit problem and satisfies the non-mixing requirement:

The Multi-Material Model in general produced results that seemed to optimize the heat transfer. The driving force of the designs was the maximization of the length of the channels, under the pressure constraint, that kept the designs from having an infinitesimal width. Furthermore the designs made full use of the design space which was shown to be optimal (see section E). Some noteworthy points from the resulted designs of the model are discussed below:

Zero thickness interface wall: The model creates an interface wall of one dimension lower than the problem; i.e. in a 2D problem the interface wall is a line, and in a 3D problem, a surface. The optimization problem does not take into account any structural constraints and as a result the design might not be able to withstand the pressure, or maintain its shape during operation.

Manufacturability: The 3D results illustrated solid regions that are "hovering" in space. In order to produce any meaningful manufacturable designs, the design was subjected to post-processing. The resulted topology was filtered, by considering the areas where the velocity was close to zero to be solid.

Parasitic heat flux: In relatively low Peclet number flows, the temperature boundary condition at the inlets conducted heat to the system. As a result more thermal energy exited the system by advection than entered, by advection only. This issue was circumvented by adding low conductive extensions to the inlets.

3D results: The 3D optimization problems did not produce as clear results as the 2D ones, and one of the reason is the difficulty of representing a 3D object in a 2D surface. In one of the cases the optimizer produced bi-continuous channels, that seem to comply with the principle of maximizing the surface area of the interface.

The Multi-Material model performed better in terms of heat transfer compared to conventional concentric designs. The 3D models gave an insight of how to maximize the heat transfer by generating bi-continuous structures, that can be realised with modern manufacturing processes, such as additive manufacturing. Furthermore we saw that reducing the thickness of the wall between the flows is beneficial to the heat transfer. An ideal zero thickness wall reduces the heat resistance between the two flows but in reality will not be able to withstand the pressure loads. Furthermore fin structures are not beneficial in 2D problems, as explained in appendix C.

6.2. FURTHER RESEARCH

The proposed Multi-Material Model seems to perform well in maximizing the heat transfer, but further research must be done to improve the model in five different directions:

Structural integrity: This study did not consider any structural constraints, such as the strength, the compliance of the design, etc. Currently there exist solid-fluid interaction models used for topology optimization problems that take into account structural constraints. These could be adapted for use in the studied problem.

Flow regime: This study focused on laminar flow problems, mainly for computational simplicity, and to simplify the analysis as much as possible before moving to even more complex problems. A step forward in modelling a wider range of heat exchangers would be to incorporate turbulence effects. There exist many turbulence models (for example see [29]). Moreover topology optimization problems of turbulent flows have been investigated ([28]). So extending the current work to include turbulence models is feasible.

Manufacturability: More research should be done on the 3D problems, in order to investigate how the model performs in different geometries, velocities, and fluids. Furthermore the post-processed designs must be tested on how they perform.

Fouling: An important aspect in the design of heat exchangers that has not taken into consideration is the fouling of heat exchangers. Fouling happens by deposition of material on the walls of heat exchangers, reducing the ability to efficiently transfer heat, as well as increasing the pressure drop of the system. As a future work it is proposed to include a fouling factor, in order to get a more realistic correlation of heat transfer.

Convergence: The order of the polynomial of the interpolated permeability influences the convergence of the optimization problem, leading to suboptimal designs. There is no clear understanding of this effect and further research must be done to establish causality.

A

HAGEN–POISEUILLE FLOW DUE TO PRESSURE GRADIENT BETWEEN FIXED PLATES

We consider the two dimensional fully developed problem of laminar incompressible flow between two fixed parallel infinite depth plates. Considering the velocity vector to be $\mathbf{u} = \begin{pmatrix} u \\ v \\ w \end{pmatrix}$ the 2D Navier-Stokes equation is becomes [14]:

$$\rho\left(u\frac{\partial u}{\partial x} + v\frac{\partial u}{\partial y}\right) = -\frac{\partial p}{\partial x} + \mu\left(\frac{\partial^2 u}{\partial x^2} + \frac{\partial^2 u}{\partial y^2}\right) + \rho g_x. \tag{A.1}$$

If we don't take into account gravity, and considering $v = w = 0$ equation A.1 becomes:

$$\frac{dp}{dx} = \mu\frac{\partial^2 u}{\partial y^2}. \tag{A.2}$$

Considering the boundary condition at the plates where $u(y = \pm h) = 0$ we can find the solution of u to be:

$$u = -\frac{dp}{dx}\frac{h^2}{2\mu}\left(1 - \frac{y^2}{h^2}\right). \tag{A.3}$$

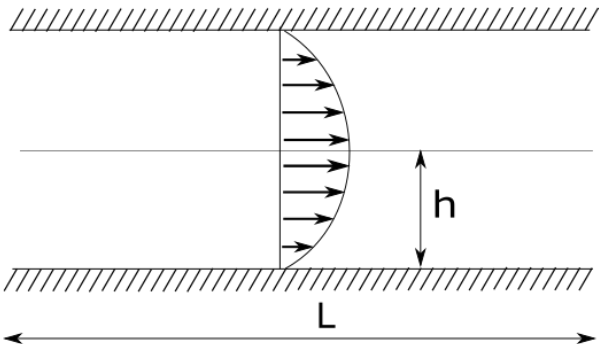

Figure A.1: Parabolic velocity profile of Hagen–Poiseuille flow

B

SENSITIVITY ANALYSIS

Sensitivity analysis is the study of how the output, in our case the objective function $H(\mathbf{x},\mathbf{u})$, changes with the perturbation of the design variables $\mathbf{x}$. In other words we are interested in finding out the derivatives of the objective function with respect to the design variables: $\frac{dH}{d\mathbf{x}}$.

B.1. ADJOINT METHOD

In general the system of equations of a problem can be written in the form of a linear system of equations, $\mathbf{Ku} - \mathbf{b} = \mathbf{r} = \mathbf{0}$. Then the state derivatives $\frac{\partial \mathbf{u}}{\partial \mathbf{x}}$, can be expanded as follows. We introduce the Lagrangian multipliers $\boldsymbol{\lambda}$ in order to form the Lagrangian function as shown in equation B.1.

$$H^*(\mathbf{x},\mathbf{u}(\mathbf{x}),\boldsymbol{\lambda}) = H(\mathbf{x},\mathbf{u}(\mathbf{x})) - \boldsymbol{\lambda}\mathbf{r}(\mathbf{x},\mathbf{u}(\mathbf{x})). \tag{B.1}$$

The Lagrangian multiplier vector has the same size as the residual vector. The sensitivities of the new objective H^* with respect to the design variables become:

$$\frac{dH^*}{d\mathbf{x}} = \frac{\partial H}{\partial \mathbf{x}} + \frac{\partial H}{\partial \mathbf{u}}\frac{\partial \mathbf{u}}{\partial \mathbf{x}} - \boldsymbol{\lambda}\left(\frac{\partial \mathbf{r}}{\partial \mathbf{x}} + \frac{\partial \mathbf{r}}{\partial \mathbf{u}}\frac{\partial \mathbf{u}}{\partial \mathbf{x}}\right). \tag{B.2}$$

Choosing the Lagrange multipliers $\boldsymbol{\lambda}$ to satisfy B.4 we can rewrite equation B.2 to equation B.3.

$$\frac{dH^*}{d\mathbf{x}} = \frac{\partial H}{\partial \mathbf{x}} - \boldsymbol{\lambda}\frac{\partial \mathbf{r}}{\partial \mathbf{x}}. \tag{B.3}$$

$$\boldsymbol{\lambda} = \frac{\partial \mathbf{r}}{\partial \mathbf{u}}^{-1}\frac{\partial H}{\partial \mathbf{u}}. \tag{B.4}$$

For a linear system the term $\frac{\partial \mathbf{r}}{\partial \mathbf{u}}$ is the stiffness matrix $\mathbf{K}$.

C

2D FINS

In section 5.2.1 the optimized result illustrated a fin structure between the two flows, as shown in figure 5.19a. We can derive an relation for the heat transfer, analogous to an electric circuit (see figure C.1), as:

$$\dot{Q} = \frac{\Delta T}{R}, \tag{C.1}$$

where,

$\dot{Q}$ = is the power transferred between the two flows,
ΔT = is the Temperature difference between,
R = is the equivalent thermal resistance.

The equivalent total thermal resistance of the design is dependent on the resistance of the two fluids and the wall, as seen in figure C.2 and is calculated to be:

$$R = R_w + R_h + R_c, \tag{C.2}$$

where,

R_w = is resistance of the wall,
R_h = is the resistance of the hot flow,
R_c = is the resistance of the cold flow.

Furthermore,

$$R_w = \frac{L}{k_w A_w}, R_h = \frac{1}{h_h A_h}, R_c = \frac{1}{h_c A_c},$$

where,

$A_{h,c,w}$ = are interface areas of the hot flow, cold flow, and wall respectively,
$h_{h,c}$ = are convective heat transfer coefficients of the hot and cold flow respectively,
k = is the conductivity of the wall.

The convective heat transfer coefficients h_h and h_c represent how easy is the heat transferred through the flow and are dependent on the flow characteristics (Reynolds, Peclet and Prandtl numbers) and the channel's geometry.

In the optimized design the conductive of the wall was chosen to be 1000 times higher than the conductivity of the fluid, so the wall resistance is negligible compared to the rest. Equation C.2 is then equivalent to:

$$R = \frac{1}{h_h A_h} + \frac{1}{h_c A_c}. \tag{C.3}$$

Equation C.3 shows that it would be optimal to increase the surface area of both flows instead of just one, since the total resistance becomes is dominated by the most resistive element. This leads to the conclusion that this design is suboptimal if compared to a serpent like structure as the one in figure 5.10b

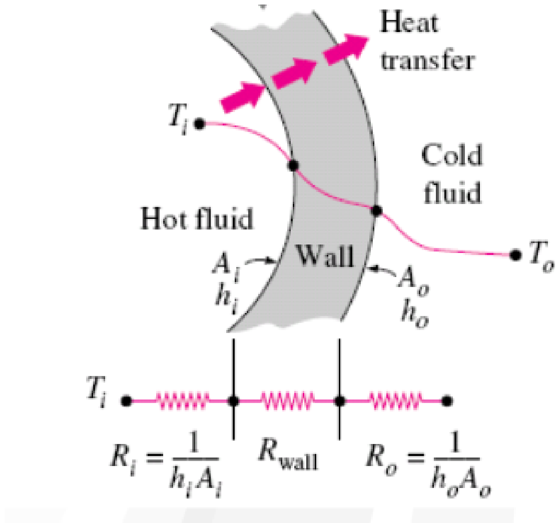

Figure C.1: Thermal circuit analogues to an electric circuit.[37]

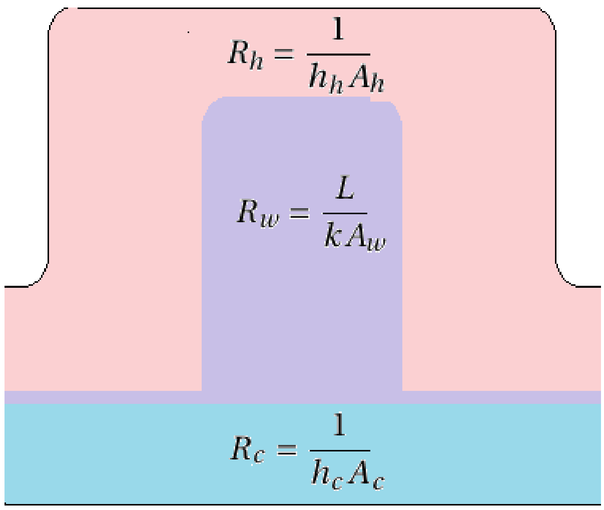

Figure C.2: Parabolic velocity profile of Hagen–Poiseuille flow

D

Optimal Wall conductivity for Counterflow Heat Exchangers

In parallel heat exchangers, the more conductive the wall is, the higher the heat transfer between the two fluids is. This is because the wall behaves as a thermal resistor between the high and low temperature fluids. But this is not the case in a counter-flow heat exchanger, where there exists an optimal wall conductivity, as we discovered while performing a single parameter optimization. This was also observed by Stief et al. [38].

To elaborate on this aspect of the counter flow heat exchangers, we performed the following experiments. We simulated a simple counter-flow, infinite deep plate heat exchanger (see figure D.1) in 2D. We varied the ration of the solid to fluid conductivity and measured the heat transfer percentage between the two fluids. We performed the simulation for two cases: for isotropic solid material, where the conductivity of the solid was the same in all directions, and for anisotropic solid material, where the conductivity in the axial direction was set to zero. We saw that if there is no axial heat transfer, the energy transferred between the two fluids monotonically increases, while in the case of the isotropic material the transferred energy maximizes at a certain ratio. Furthermore the anisotropic solid material always outperforms the isotropic one, as shown in figure D.2. A highly conductive isotropic wall will result in an almost uniform temperature profile on the wall which has a negative effect on the temperature difference between the two flows as it can be seen in figure D.1d.

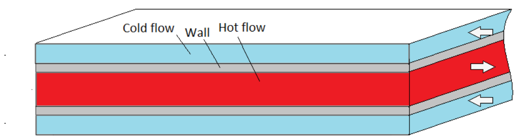

(a) Counter-flow concentric pipe heat exchanger.

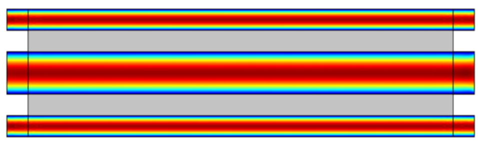

(b) Velocity field of 2D plate flow. The velocity profile is fully developed resulting in the characteristic parabolic profile.

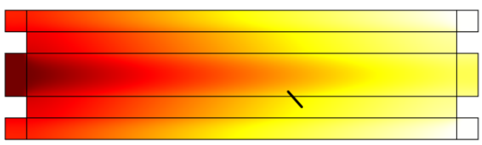

(c) Temperature field of optimal conductivity ratio.

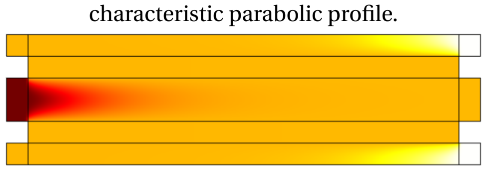

(d) Temperature field of highly conductive isotropic material.

Figure D.1: Heat transfer in counter flow heat exchanger and the effect of axial heat transfer

One might expect a design where the thermal resistivity of the interface to be maximum in the axial direction and minimum in the radial direction.

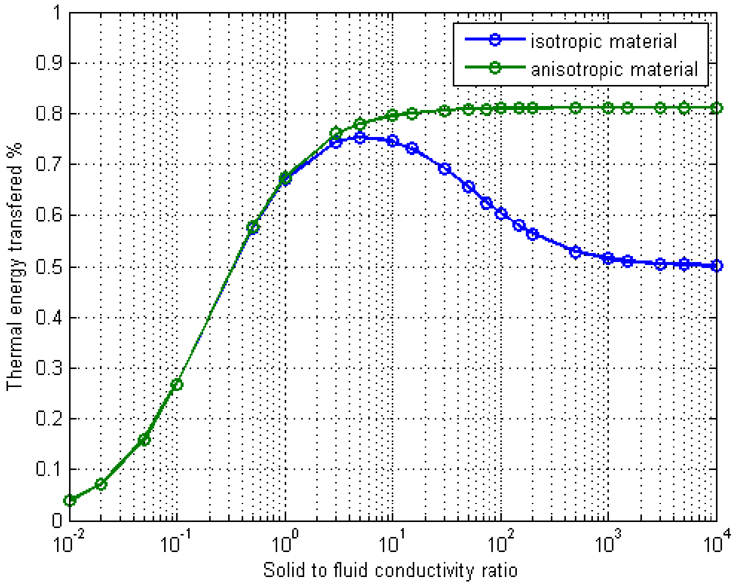

Figure D.2: Heat transfer with respect to conductivity ratio between the wall and fluid for two different fluid conductivity values. The maximum value of the transferred heat is capped by the geometric constraints, such as the finite length of the channels.

E

A BETTER UNDERSTANDING OF THE OPTIMAL DESIGN

In order to have a better understanding on how an optimal heat heat exchanger should behave, we perform a parametric study, on the width and length of the channels of a 2D heat exchanger. We consider a simplified problem such as the one shown in figure E.1. This problem is a simple laminar duct flow, better known as a Hagen–Poiseuille flow [14], coupled with convective heat transfer. A Hagen–Poiseuille flow is a laminar incompressible plane flow through infinitely deep plates (see appendix A). Such a flow is characterized by a velocity component u in only one direction.

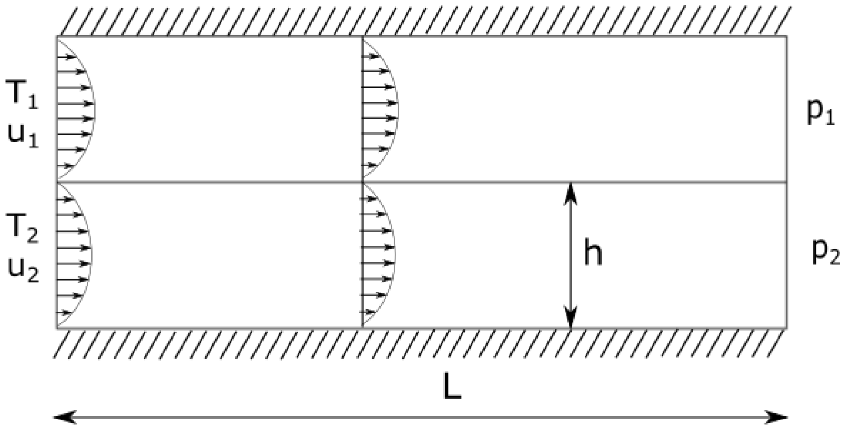

Figure E.1: Simple 2D problem of parallel flow in straight channels modelled as Hagen–Poiseuille flow.

The velocity profile of a fully developed flow can be shown to be:

$$u = -\frac{dp}{dx}\frac{h^2}{2\mu}\left(1-\frac{y^2}{h^2}\right). \tag{E.1}$$

Assuming a constant flow rate independent of the channel diameter, it is easy to show that:

$$\int_{-h}^{h} u\mathrm{d}y = \text{const.} \tag{E.2}$$

Therefore the pressure drop can be calculated to be:

$$-\frac{dp}{dx}\frac{h^2}{2\mu}\int_{-h}^{h}\left(1-\frac{y^2}{h^2}\right)\mathrm{d}y = \int_{-h}^{h} u\mathrm{d}y \Rightarrow -\frac{dp}{dx}\frac{h^2}{2\mu}\frac{4h}{3} = \int_{-h}^{h} u\mathrm{d}y \Rightarrow -\frac{dp}{dx} \sim \frac{1}{h^3} \Rightarrow,$$

$$(\Delta P)_L \sim \frac{L}{h^3}. \tag{E.3}$$

Equation E.3 shows that the pressure drop over the length of the channel is linearly dependent to the total length, and inversely proportional to the cube of the width of the channel. We already established a relation between the pressure drop and the size of the channel, so we will now establish a relation between the heat transfer and the size of the channels. We did that by means of numerical simulations.

For a varied width and length we solved the heat transfer problem shown in figure E.1 using. In figure E.3 we can see that the optimal pair of length and width lies in the intersection of the maximum allowed pressure drop and the constraint of limited design space. A limited design space constraint is taken into account by considering the following inequality:

$$2 \cdot l \cdot w \leq \int d\Omega$$

where l and w are the length and width of the channel, and Ω is the design domain. This constraint is an upper hard limit. It seems that for these specific flow characteristics the designs should always make full use of the design space and allowed pressure drop. This comes in agreement with the optimal designs seen in figure 5.11.

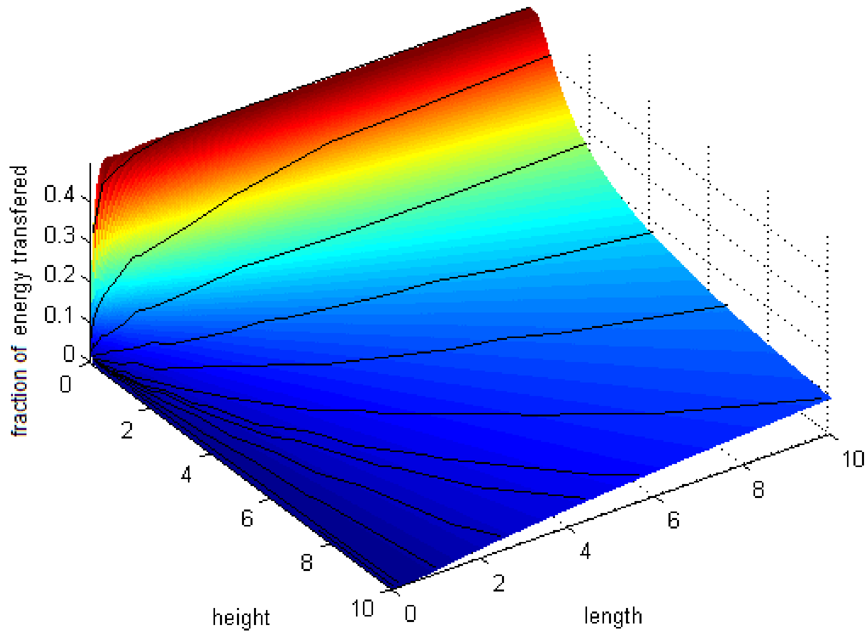

Figure E.2: Dependency of heat transfer of Hagen–Poiseuille flow. Black lines are constant pressure contours.

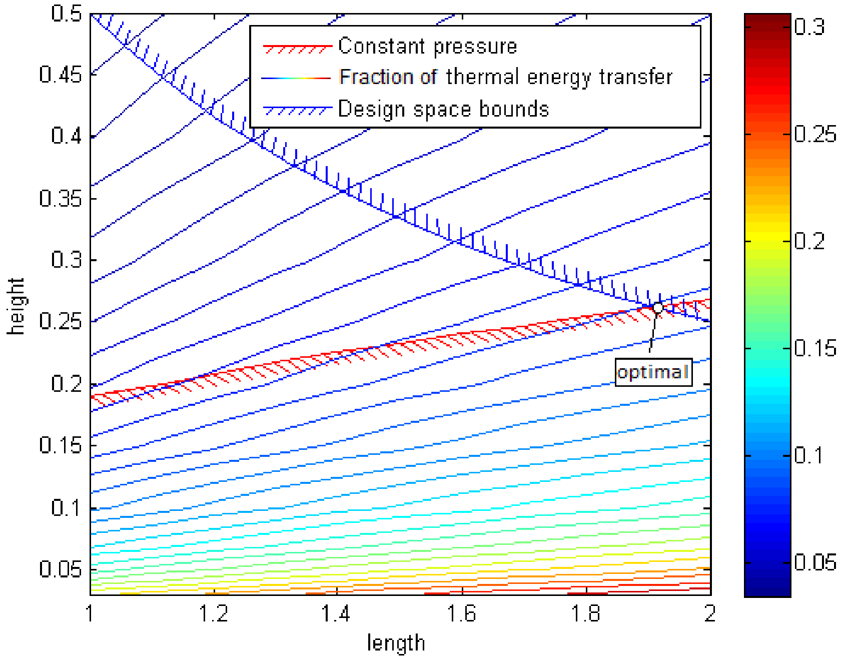

Figure E.3: Optimal length and width for Hagen–Poiseuille flow heat transfer. Optimal design makes full use of the design space.

Bibliography

[1] http://www.engineeringtoolbox.com/arithmetic-logarithmic-mean-temperature-d_436.html (accessed September 1, 2015).

[2] H. A. Navarro and Cabezas, *Effectiveness-ntu computation with a mathematical model for cross-flow heat exchangers,* Brazilian Journal of Chemical Engineering **24**, 509 (2007).

[3] S. Jain and C. Bullard, *Optimization of Heat Exchanger Design Parameters for Hydrocarbon Refrigerant Systems,* **61801** (2004).

[4] K. S. Lee, W. S. Kim, and J. M. Si, *Optimal shape and arrangement of staggered pins in the channel of a plate heat exchanger,* International Journal of Heat and Mass Transfer **44**, 3223 (2001).

[5] A. Hadidi and A. Nazari, *Design and economic optimization of shell-and-tube heat exchangers using biogeography-based (BBO) algorithm,* Applied Thermal Engineering **51**, 1263 (2013).

[6] D. Liu and S. V. Garimella, *Analysis and optimization of the thermal performance of microchannel heat sinks,* International Journal of Numerical Methods for Heat & Fluid Flow **15**, 7 (2005).

[7] C. W. B. S˙ Jain, *Optimization of heat exchanger design parameters for hydrocarbon refrigerant systems,* .

[8] M. P. Bendsoe and O. Sigmund, *Topology Optimization: Theory, Methods and Applications* (Springer, 200) p. 370.

[9] J. Alexandersen, O. Sigmund, C. Andreasen, and N. Aage, *Topology optimisation for coupled convection problems,* (2013).

[10] A. Koga, E. Lopes, and H. V. Nova, *Development of heat sink device by using topology optimization,* International Journal of Heat and Mass Transfer **64**, 759 (2013).

[11] G. Marck, M. Nemer, and J.-L. Harion, *Topology optimization of heat and mass transfer problems: laminar flow,* Numerical Heat Transfer, Part B: Fundamentals: An International Journal of Computation and Methodology (2013) **63**, 508 (2013).

[12] T. Borrvall and J. Petersson, *Topology optimization of fluids in Stokes flow,* International Journal for Numerical Methods in Fluids **41**, 77 (2003).

[13] J. F. Wendt, J. D. Anderson, and B. . Institut von Karman de dynamique des fluides (Rhode-Saint-Genèse, *Computational fluid dynamics : an introduction* (Springer, Berlin, Paris, 1992) la page de titre porte : A von Karman Institute book.

[14] F. M. White, *Book*, Vol. 17 (2009) p. 864.

[15] Q. Liu and O. V. Vasilyev, *A Brinkman penalization method for compressible flows in complex geometries,* Journal of Computational Physics **227**, 946 (2007).

[16] *Heat & Mass Transfer: A Practical Approach* (McGraw-Hill Education (India) Pvt Limited, 2007).

[17] *Heat & Mass Transfer Second Edition by A.F. Mills* (1999).

[18] G. Liu, M. Geier, Z. Liu, M. Krafczyk, and T. Chen, *Discrete adjoint sensitivity analysis for fluid flow topology optimization based on the generalized lattice Boltzmann method,* Computers & Mathematics with Applications **68**, 1374 (2014).

[19] G. Marck and Y. Privat, *ON SOME SHAPE AND TOPOLOGY OPTIMIZATION PROBLEMS IN CONDUCTIVE AND CONVECTIVE HEAT TRANSFERS,* in *OPTI 2014, An International Conference on Engineering and Applied Sciences Optimization*, edited by M. Papadrakakis, M. Karlaftis, and N. Lagaros (Kos Island, Greece, 2014) pp. 1640–1657.

[20] T. Gao, W. H. Zhang, J. H. Zhu, Y. J. Xu, and D. H. Bassir, *Topology optimization of heat conduction problem involving design-dependent heat load effect,* Finite Elements in Analysis and Design **44**, 805 (2008).

[21] Q. Li, G. P. Steven, Y. M. Xie, and O. M. Querin, *Evolutionary topology optimization for temperature reduction of heat conducting fields,* International Journal of Heat and Mass Transfer **47**, 5071 (2004).

[22] Y. Xie, Q. Li, O. M. Querin, and G. P. Steven, *Shape and topology design for heat conduction by Evolutionary Structural Optimization,* International Journal of Heat and Mass Transfer **42**, 3361 (1999).

[23] C. Zhuang, Z. Xiong, and H. Ding, *A level set method for topology optimization of heat conduction problem under multiple load cases,* Computer Methods in Applied Mechanics and Engineering **196**, 1074 (2007).

[24] A. Gersborg-Hansen, O. Sigmund, and R. Haber, *Topology optimization of channel flow problems,* Structural and Multidisciplinary Optimization (2005) **30**, 181 (2005).

[25] J. K. Guest and J. H. Prévost, *Topology optimization of creeping fluid flows using a Darcy-Stokes finite element,* International Journal for Numerical Methods in Engineering **66**, 461 (2006).

[26] L. H. Olesen, F. Okkels, and H. Bruus, *A high-level programming-language implementation of topology optimization applied to steady-state Navier-Stokes flow,* International Journal for Numerical Methods in Engineering **65**, 975 (2006), arXiv:0410086 [physics] .

[27] E. Dede, *Multiphysics topology optimization of heat transfer and fluid flow systems,* proceedings of the COMSOL Users Conference (2009).

[28] E. M. Papoutsis-Kiachagias, E. a. Kontoleontos, a. S. Zymaris, D. I. Papadimitriou, and K. C. Giannakoglou, *Constrained topology optimization for laminar and turbulent flows, including heat transfer,* EUROGEN, Evolutionary and Deterministic Methods for Design, Optimization and Control (2011).

[29] S. R. Allmaras and F. T. Johnson, *Modifications and Clarifications for the Implementation of the Spalart-Allmaras Turbulence Model,* (2012) pp. 9–13.

[30] `http://mathworld.wolfram.com/RampFunction.html` (accessed July 29, 2015).

[31] Y. C. Chang, T. Y. Hou, B. Merriman, and S. Osher, *A level set formulation of {Eulerian} interface capturing methods for incompressible fluid flows,* Journal of Computational Physics **124**, 449 (1996).

[32] D. Jacqmin, *Calculation of Two-Phase Navier–Stokes Flows Using Phase-Field Modeling,* Journal of Computational Physics **155**, 96 (1999).

[33] R. P. Fedkiw, T. Aslam, B. Merriman, and S. Osher, *A Non-oscillatory Eulerian Approach to Interfaces in Multimaterial Flows (the Ghost Fluid Method),* Journal of Computational Physics **152**, 457 (1999), arXiv:jcph.1999.6236 .

[34] F. V. J. Van Kan, A. Segal, *Numerical Methods in Scientific Computing*.

[35] `http://mathworld.wolfram.com/BoxcarFunction.html` (accessed July 29, 2015).

[36] K. Svanberg, *The method of moving asymptotes—a new method for structural optimization,* International Journal for Numerical Methods in Engineering **24**, 359 (1987).

[37] `http://cmapspublic3.ihmc.us/rid=1LV42539P-1M6QVZK-19J3/Int_calor_red_resistencias_termicas.png` (accessed September, 2015).

[38] B. T. Stief, O.-u. Langer, and K. Schubert, *Numerical Investigations of Optimal Heat Conductivity in Micro Heat Exchangers,* Chemical Engineering and Technology **21**, 297 (1999).